ACTIVE VIBRATION CONTROL OF VEHICLE SUSPENSION

Xiao Dong Li
Master of Engineering

2009-08-12

Department of Electrical and Computer Engineering
McGill University, Montreal

A thesis submitted to McGill University in partial fulfilment of the requirements of the degree of Master of Engineering

Abstract

Structure-borne noise generated by tire contact on road irregularities is a very important factor in interior vehicle noise. This kind of low-frequency noise can seriously affect the driver's concentration and passenger comfort. In order to reduce this vibration-induced noise, an active vibration control of the vehicle suspension is proposed, as opposed to acoustic noise control. Since modeling uncertainties are inevitable in characterizing the dynamics of the vibration transmission path, robust feedback controllers are considered. In this thesis, an H-infinity robust controller and a mu-synthesis robust controller are designed to reduce the vibrations using actuators acting directly on the suspension. First, closed-loop simulation results are obtained on a quarter-car suspension at the Université de Sherbrooke, showing a significant reduction in vibration. Second, simulation of the controllers is also conducted on a real car. Closed-loop test results are presented and the effectiveness of the robust feedback controllers is discussed.

Résumé

Le bruit de vibration structurelle produit par le contact des pneus du véhicule sur la surface de la route est un facteur important du bruit à l'intérieur du véhicule. Ce type de bruit à basse fréquence peut affecter sérieusement la concentration du conducteur et le confort des passagers. De manière à réduire ce bruit de vibration, un contrôle actif de vibration dans la suspension du véhicule est proposé, en contraste avec la réduction active de bruit acoustique.

Puisqu'il est inévitable d'avoir des incertitudes dans le modèle de la dynamique de transmission de la vibration, des contrôleurs rétroactifs robustes sont considérés. Dans cette thèse, un contrôleur robuste H-infini et un contrôleur à synthèse mu sont conçus pour réduire la vibration en utilisant des actionneurs agissant directement sur la suspension. En premier lieu, des résultats de simulation obtenus sur une suspension d'une seule roue à l'Université de Sherbrooke démontrent une réduction significative de la vibration. Puis, une simulation des contrôleurs est effectuée sur le modèle de la voiture. Les résultats des tests en boucle fermée sont présentés et l'efficacité des contrôleurs rétroactifs robustes est discutée.

ACKNOWLEDGEMENTS

I would first like to deeply thank my supervisor Professor Benoit Boulet for his guidance, encouragement and financial support during my master studies. Not only has he given me the academic knowledge but also he has given me invaluable support in my life.

I would like to thank Walid Belgacem and other group members at Université de Sherbrooke for their generous help in the supply of experimental equipments. PhD student Ahmad Haidar in my laboratory also gave me invaluable help during my work on my project.

Finally, I would like to thank my family for their encouragement and support during these years. I also thank my girlfriend Wei Zhang for her caring and encouragement.

TABLE OF CONTENTS

LIST OF FIGURES

LIST OF TABLES

Chapter 1 Introduction

The automobile has developed into the most important means of transportation in our lives, and passenger's comfort is one of the factors in assessing vehicle quality. Noise level inside the cabin must be considered and one of the noise sources is vibrations caused by a rough road surface.

Some work has been done on acoustic control using microphones set up inside the vehicle [1]. Some other work proposed the active control of suspension by actuator to reduce the vibration and further reduce the noise. Today, actively controlled suspensions have been installed on many luxury cars such as the Audi A8L. With the development of electronics technology, the cost of a control system becomes lower and lower and the active controlled suspension will soon be ready to be installed in most vehicles. This is one of the motivations for us to do this research.

In this thesis, a robust feedback controller is designed to suppress the vibrations in suspensions based on two different test equipments.

In Chapter 2, previous work on flexible structure modeling, uncertainty modeling and robust controller design methods is discussed, giving readers a general review of these fields.

Experimental equipment is introduced in Chapter 3. There are two equipments included: one test bench which is a quarter-car suspension system. Another one is a BUICK test car with a type of McPherson suspension. Theoretically, controllers for all four suspension systems should be designed. However, due to the time limit, only front-right suspension is considered.

Suspension Modeling is given in Chapter 4. Modal parameter identification method is used to model this dynamic system. Two equipments are modeled by different number of modes since the structures are not exactly the same. The transfer function of each mode is described by three parameters: natural frequency, damping ratio and output gains. The robust controller will be designed based on this model.

In Chapter 5, two robust controllers are designed to reduce vibrations of the suspension at the resonant peaks. Two methods are considered: H-infinity robust controller design and μ -synthesis robust controller. Simulation results and comparisons are given at the end.

In Chapter 6, the disadvantage and future work are discussed.

Chapter 2 Literature Review

Three major parts are included in this thesis: suspension system modeling, uncertainty modeling and active controller design. We will review the previous work on these three parts in the following.

2.1 Dynamic System Modeling

Various modeling methods for dynamic systems have been developed in the fields of civil engineering and mechanical engineering. This section gives a review of dynamic system modeling work in recent years.

Modal parameter identification is a very popular method used to identify flexible dynamic systems. This approach is important for the people dealing with vibration problems. In system identification, many approaches have been developed to achieve the parameter identification.

Eigensystem Realization Algorithm (ERA) proposed by Juang and Pappa [2] has been applied for modal parameter identification for dynamic systems by many researchers. ERA procedures mainly include two parts: First, a linear model for a dynamic system is realized by the use of the generalized Hankel matrix and then this model is transformed to modal parameter form. Second, by truncating some of the modes, the model can be represented in the lower order. However, after the number of modes is reduced using some provided information, the truncated model may no longer be accurate. More details about ERA are shown in reference [2]. Pappa, James and Zimmerman [3] proposed a new technology called Autonomous Modal Identification to improve ERA identification results. There is more algorithm parameters are used to implement the ERA analysis since the Hankel matrix used in [2] is varied. The Consistent Mode Indicator (CMI) can be applied to determine the confidence level for each mode. In this way, CMI effectively reduces the number of modes and improves the model accuracy. More details about CMI are found in [4].

Finite element technique is also used to extract vibration parameters from various dynamic systems. Rodriquez [5] has successfully applied this method on a rotating shaft system to model the cracked and uncracked shaft rotating. Vibration parameters of a transverse open crack on a rotating shaft are determined and vibrations of the crack are caused by the harmonic excitation force induced by an unbalanced disk. This dynamic system is divided into six elements. Narkis in [6] states that the only information required for accurate crack identification is the variation of the first two natural frequencies. Therefore, in reference [5], the first three natural frequencies of the shaft were estimated by the finite element model. The experimental results in [5] shows that the finite element method is able to describe the dynamic system within a degree of accuracy. The disadvantage of this method is that the modal parameters derived from finite element model are very sensitive to crack configuration such as crack depth and location.

2.2 System Uncertainty Modeling

As we know, any model of a physical process needs approximation, which leads to model uncertainties. Thus, uncertainty modeling is an unavoidable problem with controller design for dynamic systems. Various kinds of uncertainty models have been developed and are briefly explained in the following sections. More explanations can be found in [7].

2.2.1 Additive Uncertainty

Assume the nominal process transfer matrix is $G(s)$, and the dynamic perturbation matrix is $\Delta_a(s)$. Then, the physical process transfer matrix $G_p(s)$ can be represented by equation 2.1,

$$G_p(s) = G(s) + \Delta_a(s). \qquad (2.1)$$

The Figure 2-1 can also be used to explain this model.

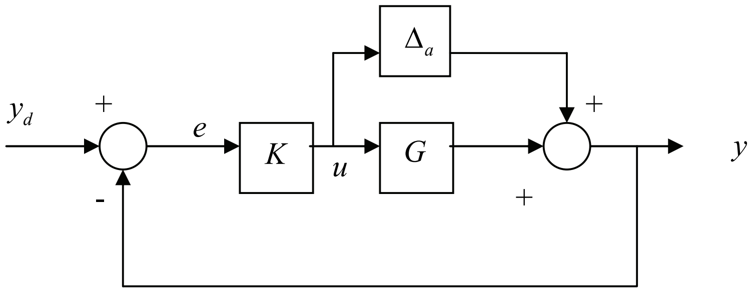

Figure 2-1: Additive Uncertainty

2.2.2 Output Multiplicative Uncertainty

Assume the nominal process transfer matrix is $G(s)$, the dynamic perturbation matrix is $\Delta_m(s)$, and the physical process transfer matrix is $G_p(s)$, then the multiplicative uncertainty taken at the output of the system can be represented by equation 2.2,

$$G_p(s) = (I_p + \Delta_m(s))G(s)\,. \qquad (2.2)$$

Figure 2-2 shows this model.

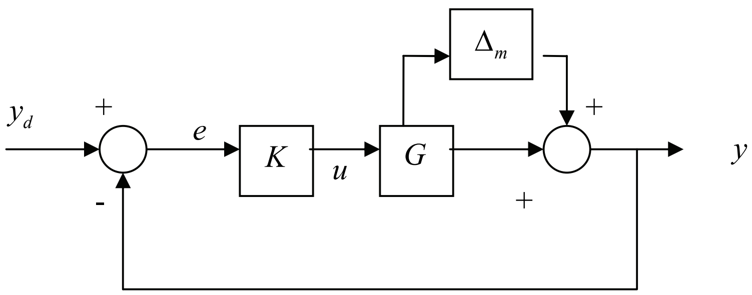

Figure 2-2: Multiplicative Uncertainty

2.2.3 Input Inverse Multiplicative Uncertainty

When the uncertainty is in the denominators of the actuator transfer functions, the input inverse multiplicative uncertainty can be considered as shown in Figure 2-3. The mathematical representation is given by

$$G_p(s) = (I_p + \Delta_{is}(s))^{-1} G(s)\,. \quad (2.3)$$

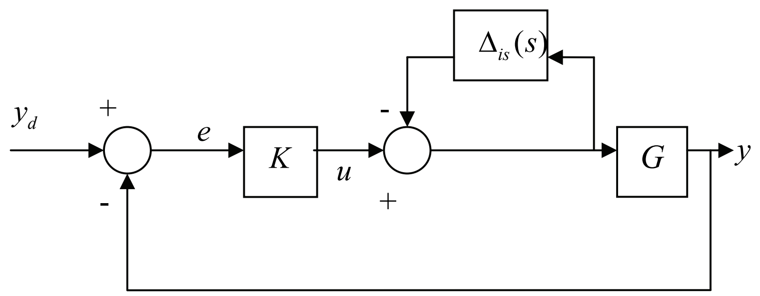

Figure 2-3: Input Inverse Multiplicative Uncertainty

2.2.4 Output Inverse Multiplicative Uncertainty

The mathematical representation o fan output inverse multiplicative uncertainty is given by

$$G_p(s) = G(s)(I_m + \Delta_{im}(s))^{-1}, \quad (2.4)$$

where $\Delta_{im}(s)$ refers to the inverse multiplicative uncertainty.

Figure 2-4 shows a block diagram representation of output inverse multiplicative uncertainty.

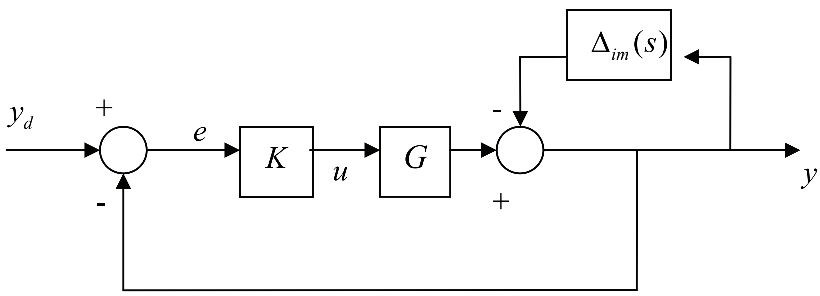

Figure 2-4: Output Inverse Multiplicative Uncertainty

2.2.5 Feedback Uncertainty

Assume that the nominal process transfer matrix is $G(s)$, and the dynamic perturbation matrix is $\Delta_f(s)$. Then, the physical process transfer matrix $G_p(s)$ can be represented by equation 2.5,

$$G_p(s) = [I_p + G(s)\Delta_f(s)]^{-1}G(s). \qquad (2.5)$$

Figure 2-5 shows the feedback uncertainty model.

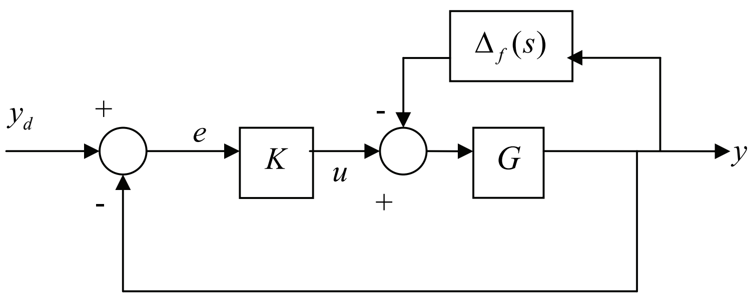

Figure 2-5: Feedback Uncertainty

2.2.6 Linear Fractional Uncertainty

Assume that the nominal process transfer matrix is $G(s)$, and the dynamic perturbation matrix is $\Delta_l(s)$. Then, the physical process transfer matrix $G_p(s)$ can be represented by equations 2.6 & 2.7,

$$G_p(s) = F_U[P(s), \Delta_l(s)] = P_{22}(s) + P_{21}(s)\Delta_l(s)[I - P_{11}(s)\Delta_l(s)]^{-1} P_{12}(s), \qquad (2.6)$$

$$\text{where } P(s) = \begin{bmatrix} P_{11}(s) & P_{12}(s) \\ P_{21}(s) & P_{22}(s) \end{bmatrix}. \qquad (2.7)$$

Figure 2-6 shows a representation of linear fractional uncertainty.

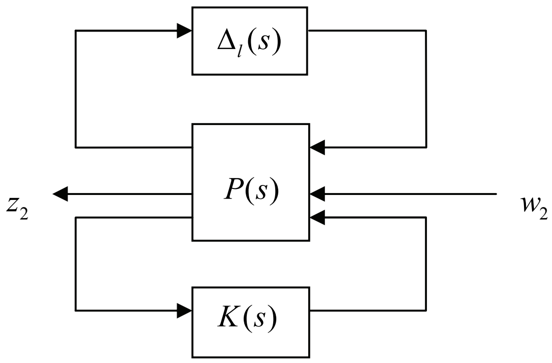

Figure 2-6: Linear Fractional Uncertainty

2.3 Robust Controller Design

Robust control is a control theory that explicitly deals with model uncertainty. This kind of controller can effectively achieve the tradeoff problem between performance and robustness, even if there exists, differences between the mathematical model and the true plant.

A variety of robust controller design methods have been developed during the last several decades. Nyquist and Bode methods were used to design fairly robust controllers in the early days. Robertsor, Leithead and O'Reilly [8] state the robust controller design by means of Nyquist and Bode analysis. The neighborhood of the relative uncertainty is plotted on the inverse Nyquist diagram and the point (-1, 0) on the inverse Nyquist plot is used to indicate the system's robustness. Residual gain and phase margins are defined on the Nyquist plot and used to indicate gain and phase margin reduction, respectively. The gain and phase robustness curves can be made to indicate the stability margin for the nominal parameters. Gain and Phase margin plots on bode diagrams can be used to show the impact of the uncertainties on systems. More details about Nyquist and Bode method for multiple-input, multiple-output systems are in references [9] and [10].

H_∞ Control theory is another very interesting approach used to design the robust controller. Kar, Seto and Doi present a controller design based on H_∞ robust control theory to suppress vibrations of a flexible structure [11]. The experimental results show that H_∞ controller can reduce the vibrations in the first five modes and the instability due to the high frequency modes can be avoided. Although H_∞ can effectively satisfy the robustness requirement in the frequency domain, it is hard to achieve the performance specification in the time domain. For this reason, Sato and Suzuki proposed an approach that combines H_∞ design with eigenstructure assignment to reduce the vibrations of flexible structures in [12]. Eigenstructure assignment method can effectively attain the desired response in time domain by full state feedback law; however, it is hard to achieve the robustness requirement in frequency domain. Obviously, by combining these two methods mentioned in [12], not only can vibrations of the flexible structure be reduced, but also the instability phenomena can be effectively avoided.

μ-synthesis robust control design has been developed for robust control system design. The advantage of μ-synthesis is that it is not only able to satisfy robust stability requirement but also achieve robust performance. μ-synthesis has been widely applied on the flexible and suspension control system design. Fujita, Namerikawa, Matsumura and Uchida apply the μ-synthesis theory to design an active robust controller for an electromagnetic suspension system in [13]. The additive uncertainty model is employed and a performance weighting function is defined. The goal is to find a controller to achieve both closed-loop system internal stability and a weighted sensitivity function that satisfies the performance requirement for all possible uncertainties. In this process, D-K iteration is used to compute the controller K. Moser [14] also propose the μ-synthesis theory to design a robust controller for flexible structures and do the experiment based on the Caltech Flexible Structure (CFS). As expected, the experimental results can effectively trade off both robust stability and performance characteristic.

Chapter3 Description of Experimental Systems

The objective of this chapter is to present two equipments used in this project: a quarter-car suspension test bench and a test vehicle. Both of them are located at Université de Sherbrooke.

3.1 Car Suspension Test Bench

A quarter-car suspension test bench mounted on a rigid structure is used to simulate a real car suspension system, shown in Figure 3-1. This test bench includes one wheel, one spring, one damper and one A-arm. This type of suspension is usually called McPherson Suspension which is very popular in modern vehicle suspension designs. An electro-dynamic shaker, Figure 3-2, together with its power amplifier, is used to simulate a realistic rough road noise excitation and is located under the wheel spindle. The dynamic shaker is also used as an actuator for the control problem. Therefore, the signal to the dynamic shakers is the sum of the input disturbance and the control signal. Nine sensors are set at different locations of the test bench to collect the experimental data in time domain. These data are then used to do the modeling and identify the uncertainty in the system. Two 3-axial sensors are located at the position 1 and 2 on the base of the suspension. Three 1-axis sensors, Figure 3-3, are located on the top of the damper, and they are positioned in such a way to measure the forces in all three directions.

A dSPACE real-time system is used to receive the signals from nine sensors and compute the control signal for the actuator. One signal conditioner is applied to convert the outputs measured by force or acceleration to electrical voltages. Several filters are also used to prevent signal aliasing. These signal processing equipment is shown in Figure 3-4.

Figure 3-1: Test Bench

Figure 3-2: Dynamic Shaker

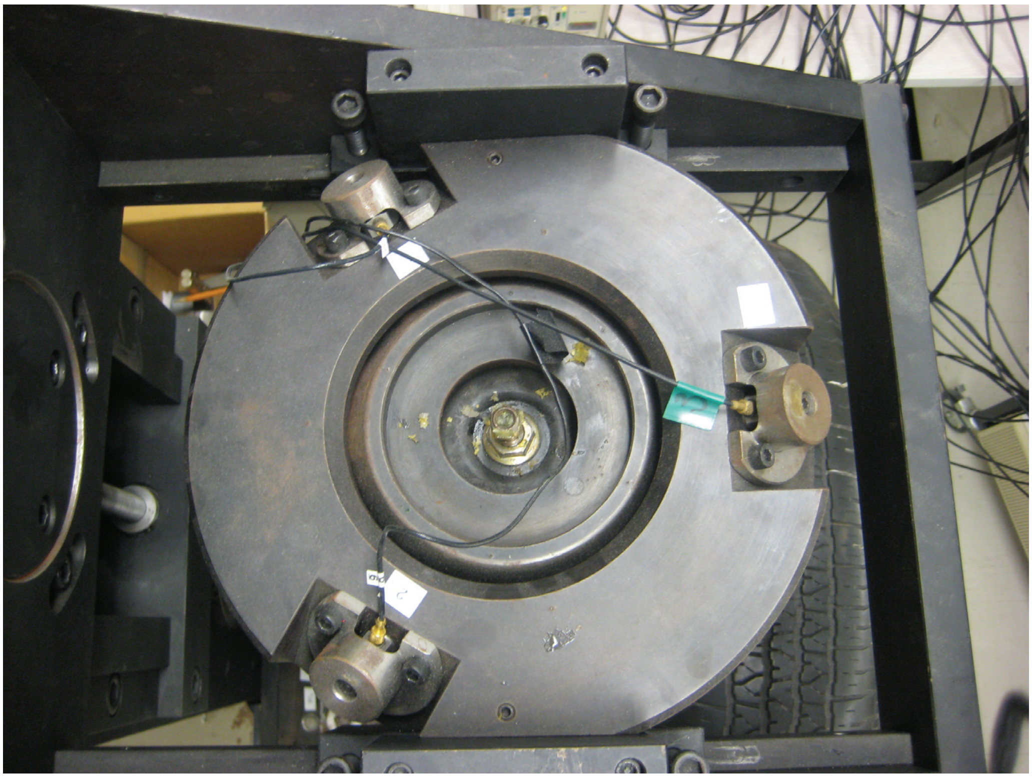

Figure 3-3: Head of the Suspension

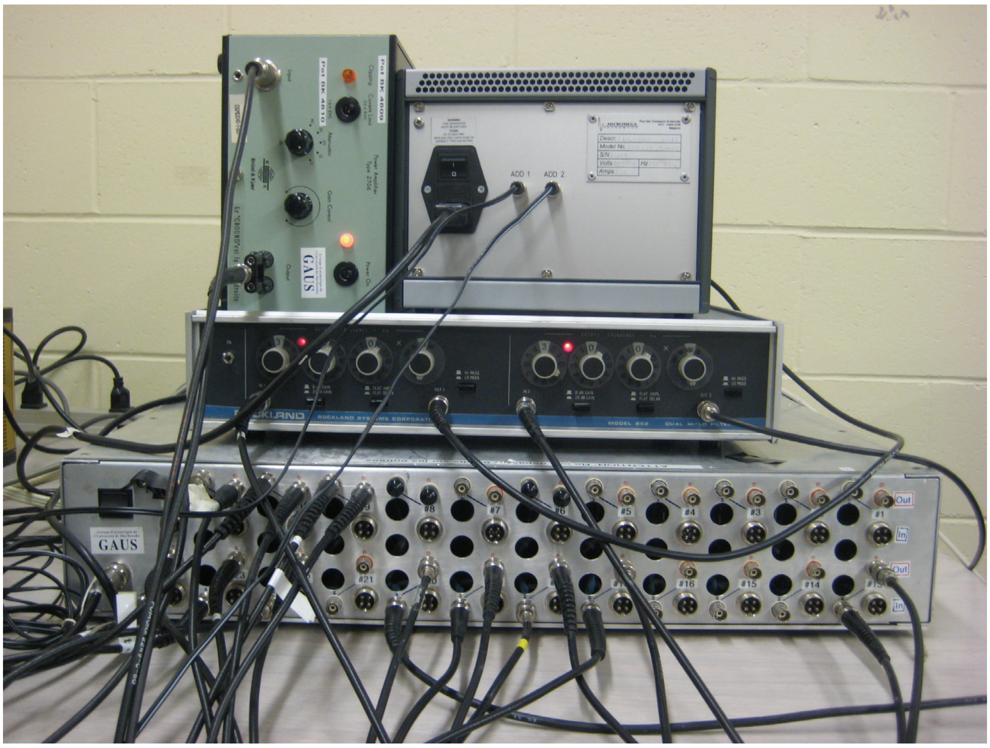

Figure 3-4: Signal Processing Equipment

3.2 Test Vehicle

To further verify the method of robust controller design on real vehicle suspension, a BUICK car, shown in Figure 3-5, is used to do the suspension modeling and controller design instead of the test bench at Université de Sherbrooke. The similar dynamic shaker, actuator and sensors are placed in each of four suspensions. At this moment, since there is no experimental data available for the other three suspensions, we only model and design the right passenger side suspension. In this process, the isolated actuator can be used to implement the control design. Due to the lack of experimental response data (secondary response) from the input of the actuator to the outputs at the time when this project started, there was no way to model the secondary path, therefore, we still used the same control technology as the one used in test bench, i.e., the dynamic shaker is used for both input disturbance generator and actuator. The suspension type is still the McPherson Suspension. As shown in Figure 3-6, the dynamic shaker is placed on the top instead of bottom of the wheel spindle in order to reduce the vibration effect on the wood platform which could then further affect the wheel tire. Nine sensors are placed at the same locations as the Test Bench. Two 3-axial sensors are located at the position 1 and 2 on the base of the suspension. Three 1-axis sensors are located on the top of the damper, and they are positioned in such a way to measure the forces in all three directions.

All of the signal processing equipment such as dSPACE system, signal conditioner and filters are also the same as the ones used for Test Bench and are shown in Figure 3-7.

Figure 3-5: Experimental Vehicle: BUICK

Figure 3-6: Dynamic Shaker

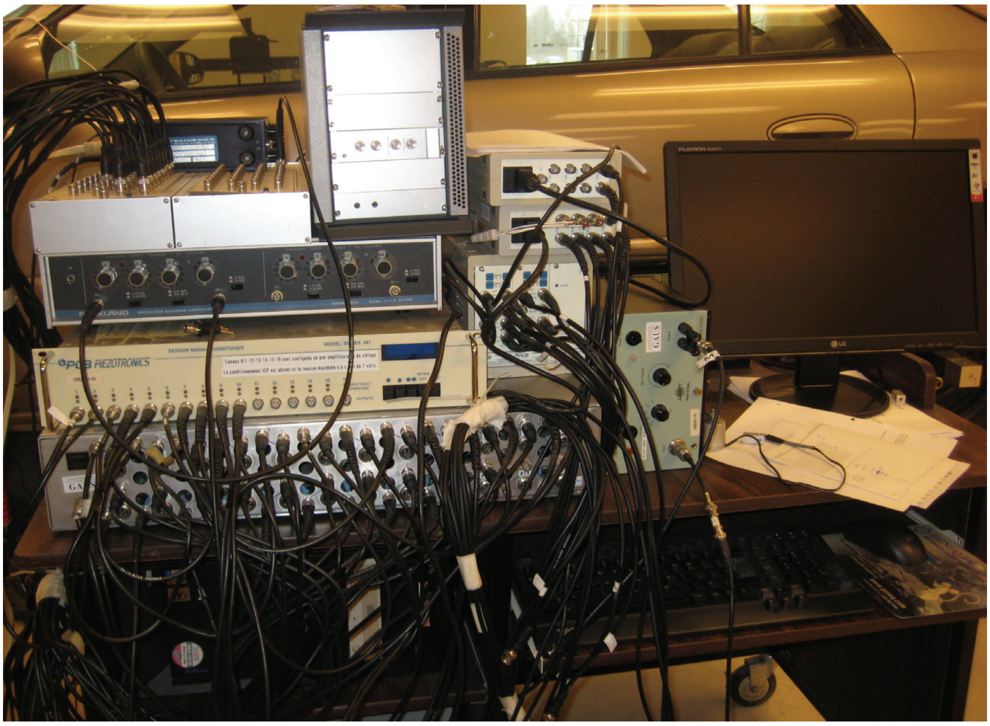

Figure 3-7: Signal Processing Device

Chapter 4 State-Space Model Identification

4.1 System Modeling

We reduce the vehicle's vibrations by reducing the vibration amplitude at each peak resonant frequency. Therefore, the suspension needs to be modeled at these resonant frequencies and the model at each resonant frequency is called a mode. A natural frequency ω_n, a damping ratio ζ and amplitude R are used to define a mode of resonance. The transfer function applied to model a mode of resonance is called receptance transfer function (4.1).

$$H(s) = \frac{R}{\omega_n^2 + s^2 + 2\zeta\omega_n s}. \tag{4.1}$$

Both the input and output signals are measured as forces. The number of modes needed is really dependent on the particular system. In our case, the test bench needs 22 modes and the test vehicle system needs 24 modes.

4.2 Experimental Data Collection

4.2.1 Data Collection in Time Domain

For the test bench, the dynamic shaker generates white noise at a maximum frequency of 1000 Hz for 10 seconds. Only one trial is conducted. For the test vehicle, the dynamic shaker generates chirp signals at a frequency range of 20-500 Hz for a period of 5 seconds. Also, one trial is conducted. For both, the output data is collected from the sensors at a sampling frequency of 1000 Hz by the dSpace system.

4.2.2 Data Collection in Frequency Domain

The experimental data in the frequency domain is obtained from the time domain. The algorithm used to compute frequency response functions is the same for both the test bench and the test vehicle. The discrete time-domain data is converted to the discrete frequency domain through the Fast Fourier Transform (FFT). However, the FFT is only working for single-input and single-output system and our system is single-input and multiple-output. Fortunately, the nine sensors are working independently; therefore, we can compute the FFT for each sensor like nine single-input, single-output systems. Assume a discrete-time signal $x[n]$ in the time domain, then the discrete Fourier transform of $x[n]$ is given by:

$$X(k) = \sum_{i=0}^{N-1} x(i) e^{\frac{-2j\pi ik}{N}} \quad . \qquad (4.2)$$

$U(k)$, the input signal in the frequency domain and $Y(k)$, the output signal in the frequency domain can be computed using equation (4.2). Power spectral densities and cross-spectral densities are derived from FFTs. Let

$$\omega_k := \frac{2\pi k}{N}, \qquad (4.3)$$

Input Auto-Spectrum: $\hat{S}_{uu}(j\omega_k) = \frac{1}{T}U(k)U(k)$, (4.4)

Output Auto-Spectrum: $\hat{S}_{yy}(j\omega_k) = \frac{1}{T}Y(k)Y(k)$, (4.5)

Input Output Cross-Spectrum: $\hat{S}_{uy}(j\omega_k) = \frac{1}{T}U(k)Y(k)$, (4.6)

Output Input Cross-Spectrum: $\hat{S}_{yu}(j\omega_k) = \frac{1}{T}Y(k)U(k)$. (4.7)

The FRFs can be obtained by equation (4.8):

$$H(j\omega_k) = \frac{\hat{S}_{yy}(j\omega_k)}{\hat{S}_{yu}(j\omega_k)}. \quad (4.8)$$

A measure of the accuracy of each individual frequency response at each discrete frequency is provided by the coherence function (4.9) as follows:

$$\gamma^2 = \frac{H(j\omega_k)}{\bar{H}(j\omega_k)} , \quad (4.9)$$

where

$$\bar{H}(j\omega_k) = \frac{\hat{S}_{uy}(j\omega_k)}{\hat{S}_{uu}(j\omega_k)}. \quad (4.10)$$

The value of coherence is between 0 and 1. When $H(j\omega)$ and $\bar{H}(j\omega)$ are similar, the coherence is close to 1, signifying that the FRFs are accurate. In this project, we obtained the FRFs from the research team working on the same system at Université de Sherbrooke.

4.3 Model Identification

An algorithm has been developed for model identification by Marie-Pierre Jolicoeur [15] and we further modified this algorithm to get a more accurate model for the test bench and real experimental car suspension system. We tried to find more accurate values for the modes, damping ratios and output gains for receptance transfer functions. This modified algorithm can be used to curve fit the experimental frequency responses more accurately and produces a complicated model such as a 24-mode suspension system in the form of a receptance transfer function. However, the disadvantage is that the new algorithm is more complicated and the computer needs longer time to run. The detailed procedure is as follows.

4.3.1 Three Parameters Identification

A frequency sweep based on the experimental frequency response is performed to identify dominant natural frequencies for each transmission path. By the previous work, the modes due to the suspension system can be distinguished from that of the rest of the test bench or vehicle such as wheels or windows. Based on this information, the frequency range that we are interested in can be defined. In this project, frequency range from 60 to 250 Hz is chosen for suspension modeling for both test bench and vehicle.

4.3.1.1 Natural Frequency Identification

The modes are identified by visually observing the peak values of the FRFs based on the FRFs from all 9 output sensors for test bench and vehicle respectively. After many trials, the natural frequency found based on the Z axis of the base sensor 2 is acceptable for all nine transmission paths of the test bench and twenty two modes are shown in Table 4-1; the natural frequency found based on the Y axis of the head sensor is the best for all nine transmission paths of the experimental vehicle and twenty four modes are shown in Table 4-1.

4.3.1.2 Damping Ratio and Output Gains Identification

As said before, we used the receptance function (4.1) to fit the experimental FRFs. Since twenty two and twenty four modes are used for test bench and vehicle respectively, the receptance functions can be expressed as

$$H(j\omega) = \sum_{i=1}^{22} \frac{R_i}{\omega_{ni}^2 - \omega^2 + 2j\zeta_i\omega_{ni}\omega} , \tag{4.11}$$

for the test bench and

$$H(j\omega) = \sum_{i=1}^{24} \frac{R_i}{\omega_{ni}^2 - \omega^2 + 2j\zeta_i\omega_{ni}\omega} . \tag{4.12}$$

for the test vehicle. Thus, our objective is to find three parameters: ω_{ni}, ζ_i and R_i to best approximate the experimental FRFs in each case. The experimental frequency response $E(j\omega)$ to be fitted is the average of all trials collected from each output. Since there is only one trial in our case, the average turns out to be the single FRF.

The most accurate parameters are found by means of the trial and error. First, by trials, we set three ranges, one for each of three parameters respectively, and also three step sizes for each scale number. Therefore, a model candidate family $H_c(j\omega)$ has been setup, and then a Matlab program is run to test different parameters and compare the model obtained, $H_c(j\omega)$ to the experimental response $E(j\omega)$. An accurate model would be obtained if the candidate family $H_c(j\omega)$ is defined properly.

The error between the frequency response of each model in family $H_c(j\omega)$ and the experimental frequency response $E(j\omega)$ is computed by the 2-norm to represent the difference between these two response. Our objective is to minimize the difference by the curve-fitting procedure. The error is defined by (4.13).

$$Error = \sqrt{\sum_{\omega=\omega_{first}}^{\omega_{last}} |E_i(j\omega) - H_p(j\omega)|^2} \qquad (4.13)$$

where i is the i^th experiment.

The curve-fitting procedure is run to find the minimum error between all candidate models and the experimental response as follows:

In this thesis, the natural frequencies ω_{ni} are set to 22 modes for test bench and 24 modes for test vehicle, and the damping ratios ζ_i and gains R_i are initially set to 0.01 and 30 respectively for both the test bench and the vehicle. If all combinations of parameters were used to compute models and compare them to the experimental FRFs, it would need a huge number of computations and take a long time to implement. For this reason, the whole curve-fitting procedure is processed mode by mode. For example, only the parameters for the first mode are varied and the error in the whole frequency range is computed for each set of parameters. The parameters corresponding to the smallest error for this particular mode are selected. Then, we move to the second mode, and the parameters for the second mode are chosen in the same way. The procedure is repeated from the first mode to the last mode and then from the last mode to the first mode. The parameters obtained from each mode are saved.

The suspension system for either the test bench or vehicle is a single-input multiple-output system, and nine transmission paths are modeled at the same time. Therefore, all of them have the same natural frequencies and damping ratios, as shown in Table 4-1, but with different gains. The gains for the test bench and vehicle are shown in Table 4-2 and Table 4-3, respectively. However, the natural frequencies and damping ratios might be different between the test bench and vehicle.

Natural Frequencies (Modes)		Damping Ratios	
Test Bench	Test Vehicle	Test Bench	Test Vehicle
70	69.82	0.3	0.02
72.93	72.75	0.075	0.28
75.38	78.61	0.13	0.145
79.78	81.54	0.05	0.16
82.72	86.43	0.08	0.055
85.66	92.77	0.095	0.115
89.08	94.73	0.05	0.04
93.49	96.68	0.125	0.115
95.94	106	0.035	0.035
97.41	107.4	0.09	0.025
99.36	111.8	0.07	0.07
110.6	112.8	0.305	0.06
131.2	131.3	0.31	0.145
153.2	139.2	0.055	0.04
156.6	141.6	0.065	0.045
165.4	152.3	0.075	0.035
180.6	158.7	0.08	0.035
190.4	161.6	0.16	0.025
213.9	174.3	0.055	0.36
221.7	178.7	0.1	0.025
230.1	180.7	0.03	0.02
240	215.3	0.11	0.055
	218.8		0.015
	224.1		0.085

Table 4-1: Natural Frequencies and Damping Ratios of the Suspension Model for Both Test Bench and Vehicle

Mode	Oput1	Oput2	Oput3	Oput4	Oput5	Oput6	Oput7	Oput8	Oput9
1	-270	705	-120	-90	-180	210	-360	255	-555
2	-465	-195	-75	-210	-510	345	480	165	405
3	900	-270	210	495	885	-870	-615	-480	-360
4	-150	30	-45	-75	-165	135	60	90	30
5	225	-300	120	225	255	-480	315	-105	180
6	-135	705	-225	-435	-135	930	-465	135	-180
7	0	-255	30	120	-30	-210	150	-15	105
8	-855	-75	210	-225	-870	120	465	450	-120
9	-15	195	-15	-45	0	135	-75	15	-75
10	915	-870	-120	450	930	-870	-15	-585	555
11	-270	420	15	-210	-300	495	-60	180	-255
12	345	930	15	15	420	165	-645	-165	-105
13	-180	-825	60	60	-615	-390	735	60	270
14	-45	105	-15	120	0	-405	-165	-45	-30
15	90	-30	30	-135	0	450	240	75	0
16	-90	-90	0	45	-90	-195	-270	-120	30
17	-75	225	45	60	-315	-510	45	-75	15
18	45	-555	-15	15	375	930	0	375	-90
19	-300	-165	315	690	-435	-870	-225	150	75
20	405	225	-645	-870	645	735	120	-825	-105
21	-315	-195	255	450	-315	-750	-120	195	-30
22	825	930	180	-675	0	915	480	330	240

Table 4-2: Gains (R_i) for different sensors of the Test Bench Model

Oput1: Base Sensor 1, X-Axis; Oput2: Base Sensor 2, X-Axis;

Oput3: Base Sensor 1, Y-Axis; Oput4: Base Sensor 2, Y-Axis;

Oput5: Base Sensor 1, Z-Axis; Oput6: Base Sensor 2, Z-Axis;

Oput7: Head Sensor, X-Axis; Oput8: Head Sensor, Y-Axis;

Oput9: Head Sensor, Z-Axis

Mode	Oput1	Oput2	Oput3	Oput4	Oput5	Oput6	Oput7	Oput8	Oput9
1	-30	-15	-15	-15	15	0	0	-30	30
2	525	360	300	240	-405	15	75	1035	-885
3	-1020	-840	-555	-405	240	-90	30	-1020	1080
4	1080	930	630	465	-105	105	-90	645	-885
5	0	-15	15	15	-135	-30	30	105	-165
6	-660	-240	-390	-270	1080	30	-75	-1020	825
7	30	60	45	45	0	-15	0	-15	-90
8	-15	-390	-90	-120	-915	45	30	525	225
9	90	90	45	45	0	-15	-15	-15	-90
10	-75	-105	-60	-45	-60	15	15	-15	90
11	540	990	330	240	1020	-75	0	600	-795
12	-405	-795	-255	-195	-1020	60	0	-540	645
13	-120	-255	150	150	435	-75	75	330	90
14	165	135	30	15	-75	15	-30	-105	60
15	-150	-135	-30	-30	-15	-15	15	15	15
16	165	120	-105	-105	-150	60	75	285	-300
17	30	0	75	60	105	-45	-30	0	195
18	15	45	-45	-45	-45	15	30	45	-180
19	-225	60	15	45	-60	90	-120	-1020	-585
20	255	150	60	30	0	-15	0	45	90
21	-240	-150	-60	-30	-15	15	0	0	-60
22	735	270	510	300	60	75	45	315	420
23	-105	-30	-15	15	-15	0	-15	-60	-60
24	-1020	-510	-1020	-750	-75	0	15	0	30

Table 4-3: Gains (R_i) for different sensors of the Test Vehicle Model

Oput1: Base Sensor 1, X-Axis; Oput2: Base Sensor 2, X-Axis;

Oput3: Base Sensor 1, Y-Axis; Oput4: Base Sensor 2, Y-Axis;

Oput5: Base Sensor 1, Z-Axis; Oput6: Base Sensor 2, Z-Axis;

Oput7: Head Sensor, X-Axis; Oput8: Head Sensor, Y-Axis;

Oput9: Head Sensor, Z-Axis

The model for base sensor 1 in the X-Axis and the head sensor in the Y-Axis are compared to the experimental data for test bench in Figure 4-1 and 4-2 respectively.

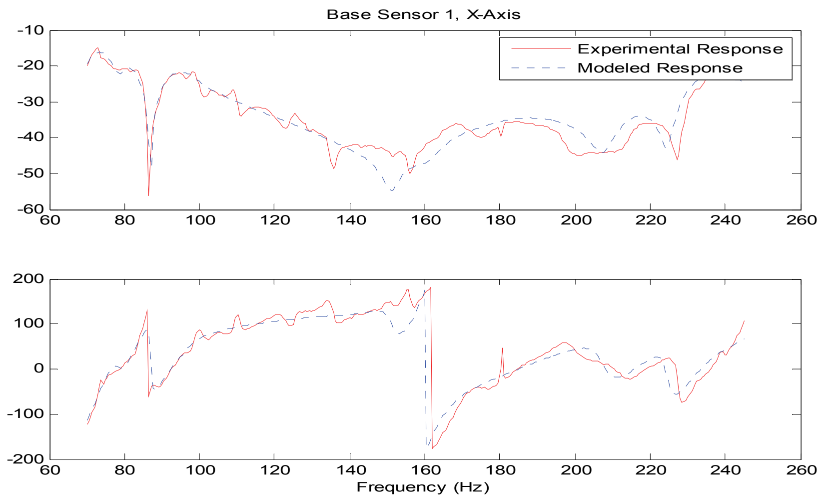

Figure 4-1: Model Response of Base Sensor 1 in the X-Axis Is Compared to the Experimental Data for Test Bench

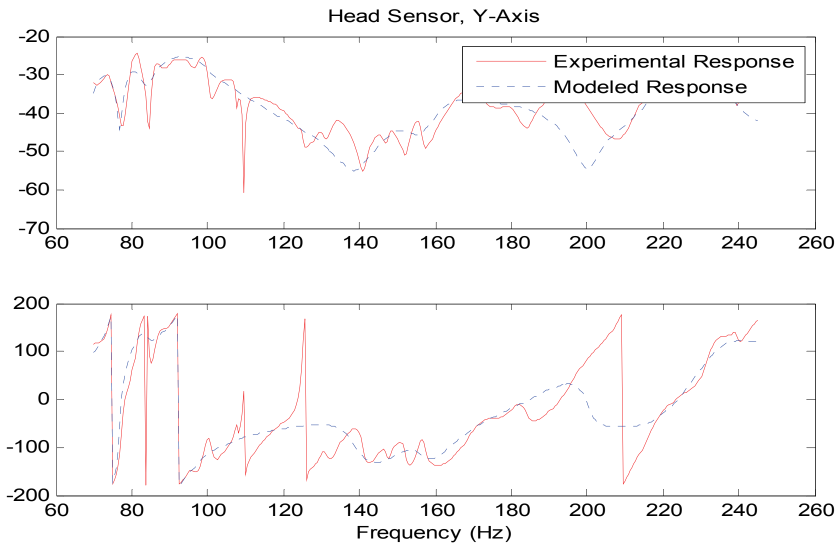

Figure 4-2: Model Response of Head Sensor in the Y-Axis Is Compared to the Experimental Data for Test Bench

The reason of more errors existing in Figure 4-2 is that the models for the sensors in different locations are built based on the resonant frequency, and the resonant frequencies are chosen in our case is more accurate for base sensor 1 other than the head sensor.

The model defined using the data from the base sensor 1 in the X-Axis and the head sensor in the Y-Axis are compared to the experimental data for test vehicle in Figure 4-3 and 4-4 respectively.

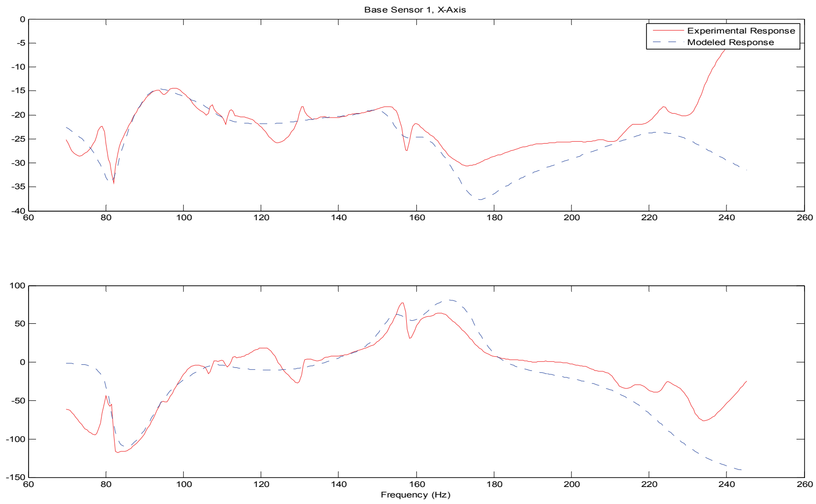

Figure 4-3: Model Response of Base Sensor 1 in the X-Axis Is Compared to the Experimental Data for Test Vehicle

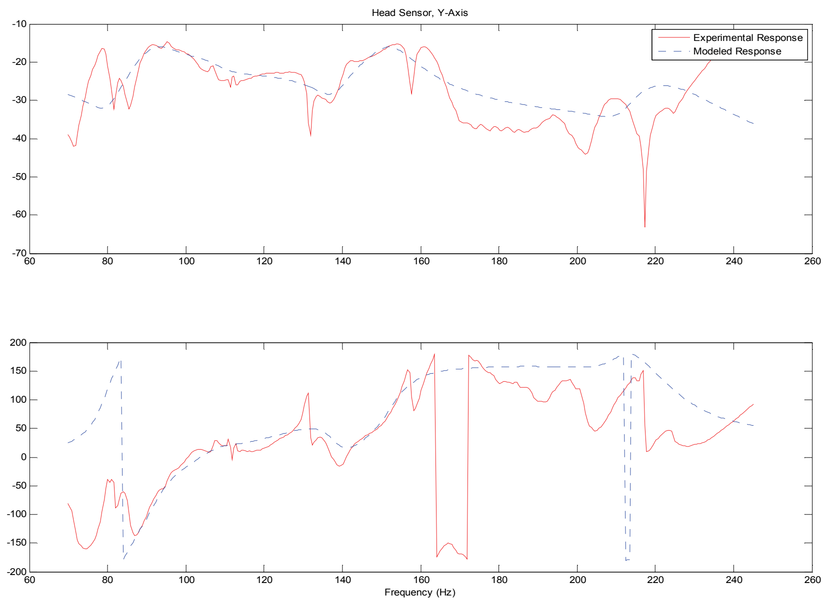

Figure 4-4: Model Response of Head Sensor in the Y-Axis Is Compared to the Experimental Data for Test Vehicle

Four Figures above show that the system can be modeled properly. And similar results are obtained for the rest of the outputs as well.

4.3.2 State-Space Form Identification

According to the conversion formula

$$H_{ss}(s) = C(sI - A)^{-1} B + D \qquad (4.14)$$

It is very easy to obtain the state-space form for the receptance transfer function. To make the problem easier, let us just think about the case of one mode and one output. In the case of one mode and one output, the dimension of the matrices are $A_{2\times 2}$, $B_{2\times 1}$, $C_{1\times 2}$, $D_{1\times 1}$. Matrix *A, B* and *C* are defined in equation (4.15), (4.16) and (4.17), respectively.

$$A = \begin{bmatrix} 0 & 1 \\ -\omega_n^2 & -2\zeta\omega_n \end{bmatrix}, \qquad (4.15)$$

$$B = \begin{bmatrix} 0 & b \end{bmatrix}^T, \qquad (4.16)$$

$$C = \begin{bmatrix} c & 0 \end{bmatrix}, \qquad (4.17)$$

$$D = 0. \qquad (4.18)$$

Therefore, by (4.14), $H_{ss}(s)$ is defined as

$$H_{ss}(s) = \frac{c \cdot b}{s^2 + 2\zeta\omega_n s + \omega_n^2}. \qquad (4.19)$$

Recall that the receptance transfer function used to model the system can be expressed as

$$H(s) = \frac{R}{s^2 + 2\zeta\omega_n s + \omega_n^2} \qquad (4.20)$$

Obviously, transfer function (4.19) will be equivalent to (4.20) if

$$R = b \cdot c. \qquad (4.21)$$

Case 1: if B and D are defined as

$$\begin{aligned} B &= \begin{bmatrix} 0 \\ 1 \end{bmatrix}, \\ D &= 0 \end{aligned} \qquad (4.22)$$

The C matrix will be

$$C = \begin{bmatrix} R & 0 \end{bmatrix}; \qquad (4.23)$$

Case 2: if B and D are defined as

$$B = \begin{bmatrix} 0 \\ R \end{bmatrix}, \qquad (4.24)$$

$$D = 0$$

The C matrix will be

$$C = \begin{bmatrix} 1 & 0 \end{bmatrix}. \qquad (4.25)$$

Actually, case 1 is equivalent to case 2. In this thesis, we choose the case 1.

For the test bench, the complete model with 22 modes and 9 outputs can be easily obtained as follows:

$$A_{44\times44} = \begin{bmatrix} \begin{bmatrix} 0 & 1 \\ -\omega_{n1}^2 & -2\zeta_1\omega_{n1} \end{bmatrix} & \cdots & 0 \\ \cdot & & \cdot \\ \cdot & & \cdot \\ \cdot & & \cdot \\ 0 & \cdots & \begin{bmatrix} 0 & 1 \\ -\omega_{n22}^2 & -2\zeta_{22}\omega_{n22} \end{bmatrix} \end{bmatrix}$$

$$B_{44\times1} = \begin{bmatrix} 0 & 1 & \cdot & \cdot & \cdot & 0 & 1 \end{bmatrix}^T \qquad (4.26)$$

$$C_{9\times44} = \begin{bmatrix} R_{1-1} & 0 & \cdot & \cdot & \cdot & R_{1-22} & 0 \\ \cdot & \cdot & \cdot & \cdot & \cdot & \cdot & \cdot \\ \cdot & \cdot & \cdot & \cdot & \cdot & \cdot & \cdot \\ \cdot & \cdot & \cdot & \cdot & \cdot & \cdot & \cdot \\ R_{22-1} & 0 & \cdot & \cdot & \cdot & R_{22-22} & 0 \end{bmatrix}$$

$$D = 0.$$

For the test vehicle, the complete model with 24 modes and 9 outputs can be easily obtained as follows:

$$
A_{48\times 48} = \begin{bmatrix} \begin{bmatrix} 0 & 1 \\ -\omega_{n1}^2 & -2\zeta_1\omega_{n1} \end{bmatrix} & \cdots & 0 \\ \cdot & & \cdot \\ \cdot & & \cdot \\ \cdot & & \cdot \\ 0 & \cdots & \begin{bmatrix} 0 & 1 \\ -\omega_{n24}^2 & -2\zeta_{24}\omega_{n24} \end{bmatrix} \end{bmatrix}
$$

$$
B_{48\times 1} = \begin{bmatrix} 0 & 1 & \cdot & \cdot & \cdot & 0 & 1 \end{bmatrix}^T \tag{4.27}
$$

$$
C_{9\times 48} = \begin{bmatrix} R_{1-1} & 0 & \cdot & \cdot & \cdot & R_{1-24} & 0 \\ \cdot & \cdot & \cdot & \cdot & \cdot & \cdot & \cdot \\ \cdot & \cdot & \cdot & \cdot & \cdot & \cdot & \cdot \\ \cdot & \cdot & \cdot & \cdot & \cdot & \cdot & \cdot \\ R_{24-1} & 0 & \cdot & \cdot & \cdot & R_{24-24} & 0 \end{bmatrix}
$$

$$
D = 0 .
$$

4.4 Uncertainty Modeling

Any mathematical representation (model) of a physical process needs approximations, which lead to model uncertainties. Due to these uncertainties, the nominal controllers may not stabilize or achieve the desired performance of the system. Hence, these uncertainties must be considered when designing the controllers. There are many ways to do the uncertainty modeling [18] such as additive uncertainty, output multiplicative uncertainty, and input multiplicative uncertainty and so on. In this thesis, the parametric uncertainty based on three parameters ω_n, ζ and R is selected since it can offer good uncertainty bounds around the nominal model. Therefore, not only the controller needs to work for the nominal model but also for the new models with the uncertainty. However, the disadvantage of working for the model with uncertainty is that the performance is also decreased. This is also the tradeoff problem between robustness and performance.

4.4.1 Parametric Uncertainty

For the uncertainty problem, we only need to consider the worst case of the uncertainty, i.e., the maximum absolute values of uncertainties. Therefore, we are going to find uncertainty bounds on the modal parameters, ω_n, ζ and R for the test bench and the test vehicle. The frequency response of the system with parametric uncertainty can be represented by equation (4.28)

$$H(j\omega) = \frac{R + \delta_R}{(\omega_n + \delta_{\omega_n})^2 - \omega^2 + 2j(\zeta + \delta_\zeta)(\omega_n + \delta_{\omega_n})\omega} \tag{4.28}$$

The variables δ_{ω_n}, δ_ζ and δ_R are the parameter uncertainties or perturbations and could be positive or negative. Obviously, there must be a family of the perturbed models called F due to different values of δ_{ω_n}, δ_ζ and δ_R. How large the perturbed family depends on the perturbation bounds. The set of the frequency responses of $F(j\omega)$ is denoted as

$$F := \{F(j\omega) = \frac{R+\delta_R}{(\omega_n+\delta_{\omega_n})^2-\omega^2+2j(\zeta+\delta_\zeta)(\omega_n+\zeta_{\omega_n})\omega}, |\delta_{\omega_n}| \le \delta_{\omega_n \max,} |\delta_\zeta| \le \delta_{\zeta \max,} |\delta_R| \le \delta_{R\max}\}$$

(4.29)

The objective is to find the family $F(j\omega)$ or $\delta_{\omega_n \max,}$ $\delta_{\zeta \max,}$ and $\delta_{R\max}$. Assume that all possible behaviours of the physical system are denoted as P. Ideally, set F should describe all of P and P should be a subset of F. However, we only have finite number of experimental data and it is impossible to know the whole P. Therefore, in this thesis, the way to solve this problem is to find a family of perturbed models F which can describe most of the experimental frequency response within some tolerance. Since it is not possible to compare the experimental response to all behaviours in F $(j\omega)$, we divide F to a finite number of subsets denoted by Fs by choosing proper step size, and then Fs is used to compare to experimental response E. Since the number of Fs is finite, it is impossible to perfectly match the experimental responses and sampled perturbed response Fs. A trial and error method is used to minimize the error between each frequency response denoted by $F_k(j\omega)$ in family of Fs and experimental response denoted by $E_i(j\omega)$. The error is computed using 2-norm and the best response denoted by $F_{min}(j\omega)$ is the one which has the minimal error with the experimental response $E_i(j\omega)$. The minimization equation is as follows:

$Minimum\{\|E_i(j\omega)-F_n(j\omega)\|_2, n=1,...,N\}$, N: the number of the candidate family

(4.30)

The minimum error is used to decide if $F_{min}(j\omega)$ is close enough to $E_i(j\omega)$. A good step to define the proper minimum error is by starting with very small bounds δ_{ω_n}, δ_ζ and δ_R. With small bounds, no $F_k(j\omega)$'s may be able to represent the physical behavior of the system. Then, bounds should be increased and the minimum error is computed again. This step is repeated until the minimum error does not have a big change and the error will be regarded as an acceptable value. Once an acceptable error is obtained, the uncertainty bounds of three parameters for experimental response $E_i(j\omega)$ are defined by $\delta_{\omega_n \exp i}{}^{\min}$, $\delta_{\zeta \exp i}{}^{\min}$ and $\delta_{R\exp i}{}^{\min}$, and the acceptable model is defined as

$$F_{\min}(j\omega) := \frac{R + \delta_{\mathrm{Re}xpi}{}^{\min}}{(\omega_n + \delta_{\omega_n \exp i}{}^{\min})^2 - \omega^2 + 2j(\zeta + \delta_{\zeta \exp i}{}^{\min})(\omega_n + \zeta_{\omega_n})\omega}, \quad (4.31)$$

All possible behaviours of the physical system for the particular $E_i(j\omega)$ can be represented by equation (4.32) in the following:

$$H(j\omega)_{\exp i} := \frac{R + \delta_R}{(\omega_n + \delta_{\omega_n})^2 - \omega^2 + 2j(\zeta + \delta_\zeta)(\omega_n + \zeta_{\omega_n})\omega}, \left|\delta_{\omega_n}\right| \le \left|\delta_{\omega_n \exp i}{}^{\min}\right| \left|\delta_\zeta\right| \le \left|\delta_{\zeta \exp i}{}^{\min}\right| \left|\delta_R\right| \le \left|\delta_{R_{\exp i}}{}^{\min}\right|$$
(4.32)

The above procedure is repeated for all experimental responses $Ei(j\omega)$, i =1,…,M. The best uncertainty bounds for all M experimental responses are expressed in (4.33), (4.34) and (4.35).

$$\delta_{\omega_n \max} = \underset{i=1,\dots,M}{Maximum}\left|\delta_{\omega_n \exp i}{}^{\min}\right|, \quad (4.33)$$

$$\delta_{\zeta \max} = \underset{i=1,\dots,M}{Maximum}\left|\delta_{\zeta \exp i}{}^{\min}\right|, \quad (4.34)$$

$$\delta_{R \max} = \underset{i=1,\dots,M}{Maximum}\left|\delta_{R \exp i}{}^{\min}\right|. \quad (4.35)$$

In order to reduce the number of comparisons between $F_k(j\omega)$ and $E_i(j\omega)$, we perform the above procedures mode by mode as in the curve fitting algorithm. Step size must be adjusted in the course of simulations. If the step size is too big, it will be hard to obtain an exact uncertainty bound. If the step size is too small, it takes a long time to simulate. Therefore, it is very important to find a balanced step size between accurate result and simulating time.

By applying this algorithm on the test bench, the uncertainties obtained for the natural frequencies, damping ratios and gains are 0.5%, 2%, and 3%, respectively. The uncertainties for the test vehicle are 0.5%, 0.9% and 0.9%.

4.4.2 Augmented State-Space Model

There exist several ways to include uncertainty to the nominal model, however, linear fractional transformation (LFT) is chosen because small gain theory can be applied for this form in a straightforward manner.

From section (4.3.2), we know that the nominal model for single mode and single output can be defined as

$$\begin{bmatrix} \dot{x}_1 \\ \dot{x}_2 \end{bmatrix} = \begin{bmatrix} 0 & 1 \\ -\omega_n^2 & -2\zeta\omega_n \end{bmatrix} \begin{bmatrix} x_1 \\ x_2 \end{bmatrix} + \begin{bmatrix} 0 \\ 1 \end{bmatrix} u$$
$$y = [R \quad 0] \begin{bmatrix} x_1 \\ x_2 \end{bmatrix}. \qquad (4.36)$$

The parameters with their uncertainties are

$$\omega_n = \overline{\omega}_n + \overline{\omega}_n \delta_{\omega_n} \Delta_{\omega_n}$$
$$\zeta = \overline{\zeta} + \overline{\zeta} \delta_{\zeta} \Delta_{\zeta} \qquad (4.37)$$
$$R = \overline{R} + \overline{R} \delta_R \Delta_R$$

where $\overline{\omega}_n$ $\overline{\zeta}$ and $\overline{R}$ are nominal values, δ_{ω_n} , δ_{ζ} and δ_R are parameter uncertainty bounds and absolute values of Δ_{ω_n} Δ_R and Δ_{ζ} are less or equal to 1, i.e. $|\Delta_x| \le 1$.

In order to embed the parameter uncertainties into the state space model and also reduce the order of the controller and make it easier to synthesize, a new uncertainty form can be represented as follows

$$\omega_n^2 = \overline{\omega}_n^2 + \overline{\omega}_n^2 \delta_{\omega_n^2} \Delta_{\omega_n^2}$$
$$\omega_n \zeta = \overline{\omega}_n \overline{\zeta} + \overline{\omega}_n \overline{\zeta} \delta_{\omega_n \zeta} \Delta_{\omega_n \zeta} \qquad (4.38)$$
$$R = \overline{R} + \overline{R} \delta_R \Delta_R$$

However, the square may increase the uncertainty bound and further affect the robust controller design in Chapter 5.

Two signals *w* and *z* are defined in equation (4.39) in order to include uncertainty into the nominal model.

$$w = \Delta z\,, \qquad (4.39)$$

with

$$\Delta = \begin{bmatrix} \Delta_{\omega_n{}^2} & 0 & 0 \\ 0 & \Delta_{\omega_n \zeta} & 0 \\ 0 & 0 & \Delta_R \end{bmatrix}, \ (4.40)$$

and

$$\|\Delta\| \le 1\ . \qquad (4.41)$$

Based on this, we can augment the model G as follows [16]:

$$\begin{aligned} \dot{x} &= Ax + B_1 w + B_2 u \\ z &= C_1 x + D_{11} w + D_{12} u \\ y &= C_2 x + D_{21} w + D_{22} u \end{aligned} \qquad (4.42)$$

More details about equation (4.42) are shown in the following:

$$
\begin{aligned}
\begin{bmatrix}\dot{x}_1\\ \dot{x}_2\end{bmatrix} &= \begin{bmatrix}0 & 1\\ -\bar{\omega}_n^2 & -2\bar{\zeta}\bar{\omega}_n\end{bmatrix}\begin{bmatrix}x_1\\ x_2\end{bmatrix} + \begin{bmatrix}0 & 0 & 0\\ 1 & 1 & 0\end{bmatrix}\begin{bmatrix}w_{\omega_n^2}\\ w_{\omega_n\zeta}\\ w_R\end{bmatrix} + \begin{bmatrix}0\\ 1\end{bmatrix}u\\
\begin{bmatrix}z_{\omega_n^2}\\ z_{\omega_n\zeta}\\ z_R\end{bmatrix} &= \begin{bmatrix}-\bar{\omega}_n^2\zeta_{\omega_n^2} & 0\\ 0 & -2\bar{\omega}_n\bar{\zeta}\delta_{\omega_n\zeta}\\ \bar{R}\delta_R & 0\end{bmatrix}\begin{bmatrix}x_1\\ x_2\end{bmatrix} + \begin{bmatrix}0 & 0 & 0\\ 0 & 0 & 0\\ 0 & 0 & 0\end{bmatrix}\begin{bmatrix}w_{\omega_n^2}\\ w_{\omega_n\zeta}\\ w_R\end{bmatrix} + \begin{bmatrix}0\\ 0\\ 0\end{bmatrix}u \qquad (4.43)\\
y &= \begin{bmatrix}R & 0\end{bmatrix}\begin{bmatrix}x_1\\ x_2\end{bmatrix} + \begin{bmatrix}0 & 0 & 1\end{bmatrix}\begin{bmatrix}w_{\omega_n^2}\\ w_{\omega_n\zeta}\\ w_R\end{bmatrix} + 0\cdot u.
\end{aligned}
$$

Thus, model G has four inputs (u and w) and four outputs (z and y), which is shown in Figure 4-5.

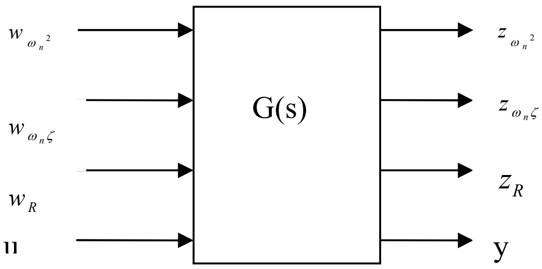

Figure 4-5: Plant G(s)

According to equation (4.39), the closed loop figure is shown as follows:

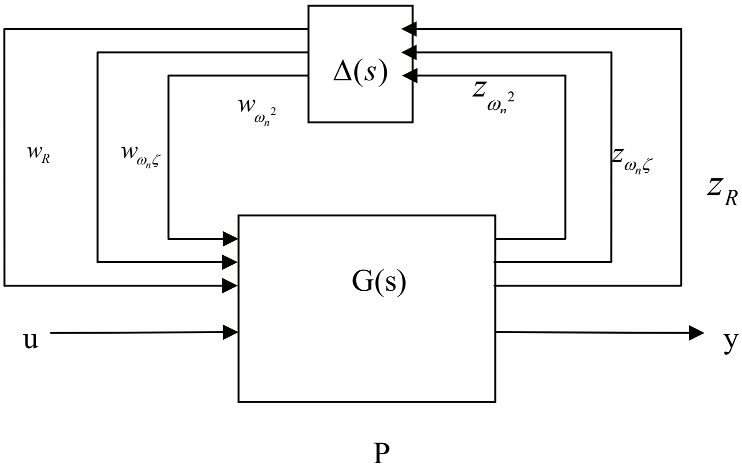

Figure 4.6: Plant P(s) $= F_u\left[G(s),\Delta(s)\right]$

This transformation form is known as the upper LFT and has the following notation.

$$P(s) = F_u\left\{G(s),\Delta(s)\right\}, \qquad (4.44)$$

With $F_u(G(s),\Delta(s)) = G_{22}(s) + G_{21}(s)\Delta(s)(I - G_{11}(s)\Delta(s))^{-1}G_{12}(s)$. (4.45)

For the test bench, there are 22 natural frequencies, 22 damping ratios and 198 gains. Hence, there are 242 parameters and 242 uncertainties. The state space system has the following dimensions: $A_{44\times44,}B_{44\times243,}C_{251\times44,}D_{251\times243}$. Since 24 modes for the test vehicle system, there are 24 natural frequencies, 24 damping ratios and 216 gains, 264 parameters and 264 uncertainties. The dimensions of the state space system are $A_{48\times48,}B_{48\times265,}C_{273\times48,}D_{273\times265}$

Chapter 5 Robust Controller Design

In this chapter, we use an output feedback closed-loop technique to reduce the vibrations of the suspension systems caused by the rough road surface. As we know, there always exist differences between the physical model and mathematical model. Thus, the controller design should not only attain a high level of performance for the mathematical model but also achieve the performance requirement for the physical system. The difference between these two models is called uncertainty, which can be represented in different types of uncertainty models. To achieve this goal, H-infinity and μ-synthesis methods are introduced in this chapter. H-infinity and μ-synthesis methods have been developed and considered as good choices for robust control of flexible structures such as vehicle suspension systems.

In the following sections, we introduce the H-infinity and μ-synthesis theory background and also its application to our design.

5.1 H-infinity Optimal Controller Design

5.1.1 H-infinity Theory

Since the H-infinity technique considers the nominal model and modeling uncertainty, a state-space equation (5.1) is used to represent the whole system [17]:

$$
\begin{aligned}
\dot{x} &= Ax + B_1 d + B_2 u \\
e &= C_1 x + D_{11} d + D_{12} u \qquad (5.1) \\
y &= C_2 x + D_{21} d + D_{22} u
\end{aligned}
$$

Where vectors d, u, e and y represent exogenous disturbances, control signals, regulated outputs and the measurements, respectively.

The state-space description can be recast into the following transfer matrix form:

$$
P(s) = \begin{bmatrix} P_{11}(s) & P_{12}(s) \\ P_{21}(s) & P_{22}(s) \end{bmatrix} = \left[\begin{array}{c|cc} A & B_1 & B_2 \\ \hline C_1 & D_{11} & D_{12} \\ C_2 & D_{21} & D_{22} \end{array}\right] \qquad (5.2)
$$

The block diagram can be shown in Figure 5-1.

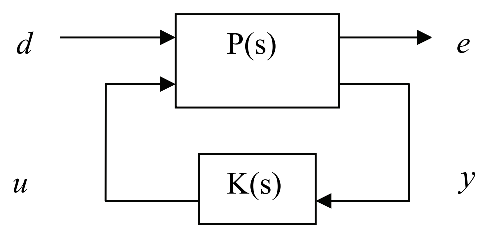

Figure 5-1: System Diagram with Robust Controller $K(s)$

In my system design, the output e represents the displacement of the suspension. Our goal is to reduce the magnitude of e when disturbance d is applied to the system. The closed-loop transfer function from the disturbances to the error is T_{ed}.

To prevent a saturation of the actuators, we should also limit the control signal u.

T_{ed} can also be written in lower LFT form such as

$$T_{ed} = F_L(P,K). \qquad (5.3)$$

It can be shown using simple algebraic manipulations that the LFT equation is given by:

$$F_L(P,K) = P_{11} + P_{12}K(I - P_{22}K)^{-1}P_{21}. \qquad (5.4)$$

The goal of H-infinity controller design is to design a stable controller $K(s)$ to minimize the H-infinity norm of the closed-loop transfer matrix, i.e., to minimize

$$\|T_{ed}\|_\infty = \|F_L(P,K)\|_\infty. \qquad (5.5)$$

The H_∞ norm of a transfer matrix is the maximum of its largest singular value over all frequencies.

$$\|T\|_\infty := \sup_{\omega \in \mathbb{R}} \bar{\sigma}\left[T(j\omega)\right] \qquad (5.6)$$

And it can also be defined as the maximum power gain of the system.

5.1.2 Suboptimal Controller

Since the optimization of equation (5.5) is very difficult to compute theoretically and numerically, instead, most software solutions use a suboptimal controller design. The general way for computing H_∞ output feedback controllers is formulated in the following way:

Given a reasonable value of γ, compute a controller K such that $\|F_L(P,K)\|_\infty < \gamma$. The value of γ is kept updating by iterative bisection procedure until reaching an acceptable error scale.

We could approximate the equation 5.2 as:

$$P(s) = \left[\begin{array}{c|cc} A & B_1 & B_2 \\ \hline C_1 & 0 & D_{12} \\ C_2 & D_{21} & 0 \end{array}\right]. \qquad (5.7)$$

In order to simplify the computation, D_{11} and D_{22} are assigned to zeros.

We also define two Hamiltonian Matrices [18]:

$$H_\infty := \begin{bmatrix} A & \gamma^{-2} B_1 B_1^* - B_2 B_2^* \\ -C_1^* C_1 & -A^* \end{bmatrix}, \qquad (5.8)$$

$$J_\infty := \begin{bmatrix} A^* & \gamma^{-2} C_1^* C_1 - C_2^* C_2 \\ -B_1 B_1^* & -A \end{bmatrix}. \qquad (5.9)$$

It is assumed that

1. The pair (A, B_1) is stabilized and the pair (A, C_1) is detectable,
2. The pair (A, B_2) is stabilized and the pair (A, C_2) is detectable,

3. $D_{12}^T \begin{bmatrix} C_1 & D_{12} \end{bmatrix} = \begin{bmatrix} 0 & I \end{bmatrix}$,

4. $\begin{bmatrix} B_1 \\ D_{21} \end{bmatrix} D_{21}^T = \begin{bmatrix} 0 \\ I \end{bmatrix}$

The H_∞ controller theorem states that there exists an admissible controller such that $\|T_{zw}\|_\infty < \gamma$ if and only if the following three conditions hold [18]:

1. $H_\infty \in dom(Ric)$ and $X_\infty := Ric(H_\infty) \geq 0$;

2. $J_\infty \in dom(Ric)$ and $Y_\infty := Ric(J_\infty) \geq 0$;

3. $\rho(X_\infty Y_\infty) < \gamma$ (The spectral radius of the product $X_\infty Y_\infty$)

When these conditions hold, one such controller is

$$K_{opt}(s) = \left[\begin{array}{c|c} \hat{A}_\infty & -Z_\infty L_\infty \\ \hline F_\infty & 0 \end{array}\right]. \quad (5.10)$$

Where

$$\begin{aligned} \hat{A}_\infty &:= A + \gamma^{-2} B_1 B_1^* X_\infty + B_2 F_\infty + Z_\infty L_\infty C_2 \\ F_\infty &:= -B_2^* X_\infty \\ L_\infty &:= -Y_\infty C_2^* \\ Z_\infty &:= (I - \gamma^{-2} Y_\infty X_\infty)^{-1} \end{aligned} \quad (5.11)$$

The schematic diagram for the H-infinity closed loop can be shown in Figure 5-2:

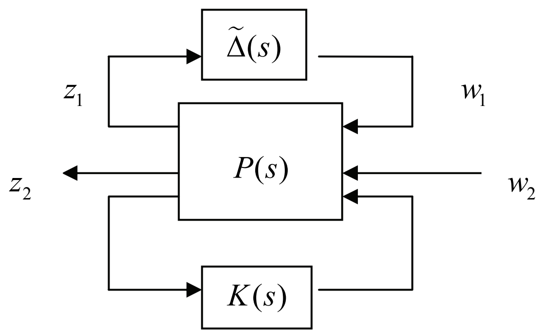

Figure 5-2: H-infinity Controller in Closed Loop

From Figure 5-2, we can see that H-infinity controller can internally stabilize the plant $P(s)$ with the uncertainty $\widetilde{\Delta}(s)$, i.e. $K(s)$ tries to minimize $\left\|T_{z_1w_1}\right\|_\infty$. However, $K(s)$ is only able to achieve the nominal performance but not robust performance, this is because it tries to minimize $\left\|T_{z_2w_2}\right\|_\infty$ which does not include any uncertainties. As we know, the goal is to minimize $\left\|\begin{bmatrix} w_1 \\ w_2 \end{bmatrix} \mapsto \begin{bmatrix} z_1 \\ z_2 \end{bmatrix}\right\|_\infty = \left\|F_L\left[P(s), K(s)\right]\right\|_\infty \leq 1$. Obviously, the $K(s)$ not only makes $\left\|T_{z_1w_1}\right\|_\infty$ and $\left\|T_{z_2w_2}\right\|_\infty$ less or equal to 1 but also makes $\left\|T_{z_2w_1}\right\|_\infty$ and $\left\|T_{z_1w_2}\right\|_\infty$ less or equal to 1. Thus, H-infinity design makes the problem more conservative than necessary. This is also known as the Mixed-sensitivity robust H_∞ controller design problem.

5.2 μ-synthesis Controller Design

5.2.1 μ Analysis

The structured singular value μ of a matrix is introduced as a tool which can be applied to analyze stability robustness with structured uncertainty in the frequency domain. The structured singular value of a complex matrix M denoted $\mu(M)$ is defined in equation 5.12.

$$\mu_{\Delta}(M) = \frac{1}{\min\{\bar{\sigma}(\Delta) : \det(I - M\Delta) = 0\}}, \text{ where } \Delta \text{ is structured uncertainty} \tag{5.12}$$

For each problem, this structure is different; it is dependent on the uncertainty Δ and performance objectives of the problem. If Δ were a full complex block, $\mu(M)$ would be equal to the maximum singular value of M. If Δ were structured, $\mu(M)$ would be upper bounded by the maximum singular value. Actually, the structured singular value is the reciprocal of the measure of the smallest perturbation Δ that destabilizes the system.

The block structure $\Gamma \subset \mathbb{C}^{n\times n}$ with $M \in \mathbb{C}^{n\times n}$ is defined as

$$\Gamma := \left\{ \Delta_s = diag\left\{ \delta_1 I_{r_1}, \ldots, \delta_q I_{r_q}, \Delta_1, \ldots, \Delta_l \right\} : \delta_i \in \mathbb{C}, \Delta_j \in \mathbb{C}^{m_j \times m_j} \right\} \tag{5.13}$$

where $r_1,\ldots,r_q,m_1,\ldots,m_l$ be positive integers such that $\sum_{i=1}^{S} r_i + \sum_{j=1}^{F} m_j = n$.

Function μ_Γ is defined as

$$\mu_\Gamma(M) := \left[\min\left\{\|\Delta_s\| : \Delta_s \in \Gamma, \det(I - M\Delta_s)\right\} = 0\right]^{-1} \qquad (5.14)$$

With complex matrix $M \in \mathbb{C}^{n\times n}$ and $\mathbb{C}^{n\times n} \to \mathbb{R}_+$.

$\mu_\Gamma(M) = 0$ when no $\Delta_s \in \Gamma$ makes $\det(I - M\Delta_s) = 0$.

The framework for the structured singular value is the same as H-infinity design except that Δ_s is structured. The interconnection of inputs, output, uncertainties and controller is shown in Figure 5-3.

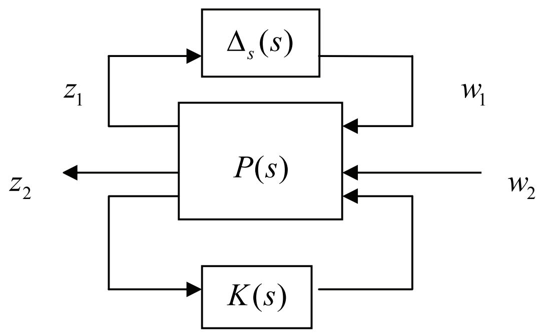

Figure 5-3: Upper and Lower Linear Fractional Transformation for μ-analysis

Robust stability with structured perturbation (Small- μ theorem):

Assume controller $K(s)$ is stabilizing for the nominal plant $P(s)$. Then given $\beta > 0$, the closed-loop system in the above figure is well-posed and internally stable for all $\Delta_s \in S$, $\|\Delta_s\|_\infty < \beta$ if and only if

$$\sup_{\omega \in \mathbb{R}} \mu_\Gamma \left\{ F_L \left[P(j\omega), K(j\omega) \right] \right\} \le \frac{1}{\beta}. \qquad (5.15)$$

Normally, the structured uncertainty is normalized, i.e. $\beta = 1$, the condition becomes

$$\sup_{\omega \in \mathbb{R}} \mu_\Gamma \left\{ F_L \left[P(j\omega), K(j\omega) \right] \right\} \le 1. \qquad (5.16)$$

As long as the condition (5.16) is achieved by μ -synthesis controller design, the closed-loop system will be robust stable for all Δ_s .

Robust Performance with structured perturbation

It is necessary to define a fictitious uncertainty Δ_p in order to achieve the robust performance requirement. The augmented Δ structure is defined as follows

$$\Omega = \{\Delta_{sa} = \begin{bmatrix} \Delta_s & 0 \\ 0 & \Delta_P \end{bmatrix} : \Delta \in \Gamma, \Delta_P \in \mathbb{C}^{n_z \times n_d}\}, \tag{5.17}$$

where Δ_P is a fictitious uncertainty which connect performance outputs to the exogenous disturbance input and it allows us to transform the robust performance problem in an equivalent robust stability problem. The configuration is shown in Figure 5-4, and this is one of the differences between μ-synthesis design and H infinity design.

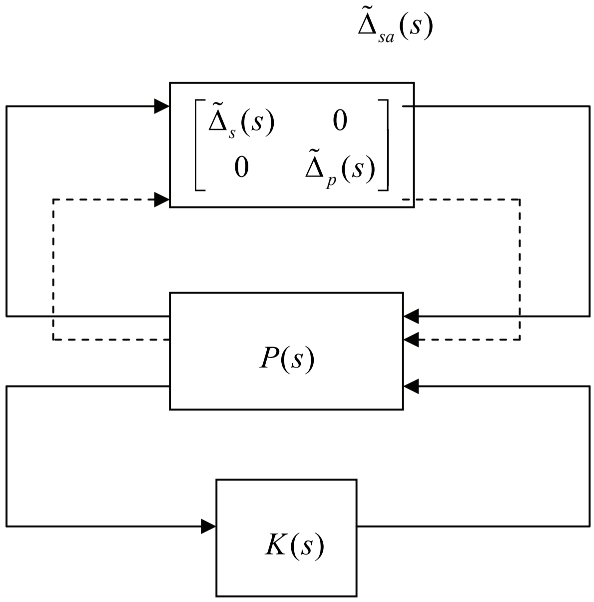

Figure 5-4: LFT Form with Augmented Uncertainty

By the theorem of Robust Performance with Structured Perturbation, we know that robust performance is achieved if and only if:

$$\sup_{\omega \in \mathbb{R}} \mu_{\Omega} \left\{ F_L \left[P(j\omega), K(j\omega) \right] \right\} \leq 1. \qquad (5.18)$$

The computation of μ is a very difficult problem. For this reason, it is more appropriate to approximate μ by its upper and lower bound. The computation procedure is as follows.

Complex structured perturbation can be defined as one unit open ball such as equation (5.19)

$$B\Gamma := \left\{ \Delta \in \Gamma : \|\Delta\| < 1 \right\} . \qquad (5.19)$$

Then $\mu_{\Gamma}(M)$ can be expressed as

$$\mu_{\Gamma}(M) = \max_{\Delta_s \in B\Gamma} \rho(M\Delta_s) , \qquad (5.20)$$

where ρ is the spectral radius.

Finally the $\mu_{\Gamma}(M)$ can be characterized by its upper and lower bound in (5.21), the proof can be found in reference [18].

$$\underset{U \in \bar{U}}{Max}\, \rho(UM) = \mu(M) \leq \inf_{D \in \bar{D}} \bar{\sigma}(DMD^{-1}) , \qquad (5.21)$$

where $\bar{U}$ is defined as $\bar{U} := \{U \in \Gamma : UU^* = I_n\}$, and $\bar{D}$ is defined as $\bar{D} := \begin{Bmatrix} diag\{D_1, ..., D_s, d_1 I_{m_1}, ..., d_{F-1} I_{m_{F-1}}, I_{m_F}\} : \\ D_i \in \mathbb{C}^{r_i \times r_i}, D_i = D_i^* > 0, d_j \in \mathbb{R}, d_j > 0 \end{Bmatrix}$.

Although equation (5.21) cannot express $\mu_\Gamma(M)$'s value directly, the lower and upper bounds are very close to each other. Thus, we can roughly compute $\mu_\Gamma(M)$ by this inequality expression, more details given in [18].

5.2.2 μ-synthesis

μ-synthesis is the robust control design counterpart of the theory of $\mu - analysis$. It is a control synthesis methodology designed to minimize the structured singular value of the augmented closed-loop system $F_l(P, K)$ in Figure 5-4. The controllers designed by μ-synthesis technique can work not only for robust stability but also robust performance. μ-synthesis is the solution to an optimization problem, equation (5.22), based on the structured singular value instead of the maximum singular value used in H-Infinity technique. Therefore, the simulation results from μ-synthesis would be less conservative than that from H_∞.

$$\min_{K(s) stabilizing} \sup_{\omega \in \mathbb{R}} \mu_\Omega \{F_L [P(j\omega), K(j\omega)]\} \qquad (5.22)$$

Recall equation (5.21), the upper bound of μ can be represented as $\inf_{D \in \bar{D}} \bar{\sigma}(DF_L(G,K)D^{-1})$. Therefore, the optimization problem can be changed to

$$\min_{D \in \bar{D}} \bar{\sigma}\left\{DF_L\left[P(j\omega), K(j\omega)\right]D^{-1}\right\}. \quad (5.23)$$

The 'dkit' function in the Matlab Mu-Analysis and Synthesis Toolbox is used to compute equation (5.23), and the process is also called D-K iteration. Implied by its name, D-K iteration proceeds by performing D and K minimization in a sequential fashion and the detailed procedure is the following [18]:

- Initialize D
- minimize $\|F_L(P,K)\|_\infty$ and finding the minimizing controller denoted by $K_{\min}$
- minimize $\bar{\sigma}\left[DF_L(P,K_{\min})D^{-1}\right]$ over D pointwise across the frequency based on the $K_{\min}$ computed in step 2, and finding a $D_{\min}$
- Compare $D_{\min}$ with D. Stop if they are close enough, or return to step 2

5.3 Weighting Functions and Matlab Setup

One of the most important steps in the robust controller design process is to choose proper weighting functions W_d, W_e, W_y, W_u. The weighting functions are included for the following reasons [18]:

- To constrain the magnitude of the input signals for actuator to avoid actuator saturation such as W_u
- To enforce closed-loop performance specifications such as W_e
- To represent the frequency contents of disturbances and noises such as W_d

To simplify our design, we only focus on the disturbance weighting function W_d, performance weighting function W_e and control signal weighting function W_u. The Matlab setup is the same for both test bench and test vehicle, and shown in Figure 5-5.

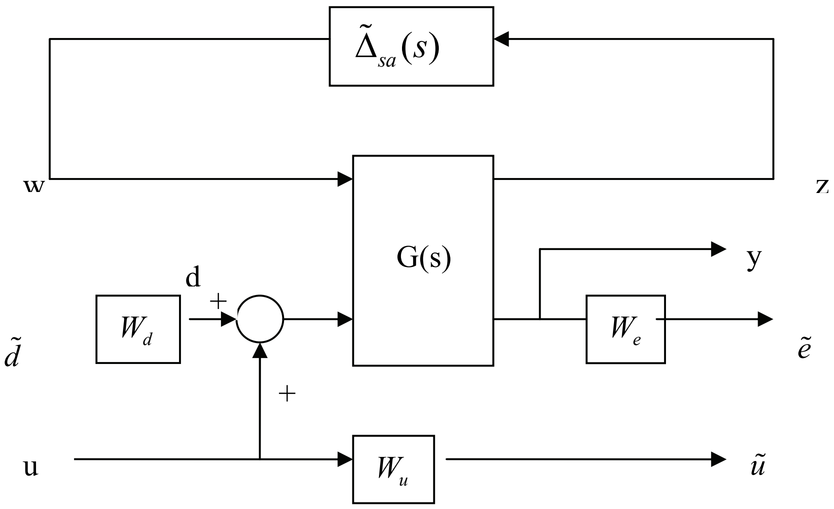

Figure 5-5: Open Loop Connections with Weighting Functions

In Figure 5-5, we can see that the dynamic shaker is used for both disturbance generator and actuator [15].

Disturbance weighting function

Since the disturbance used on the experimental test bench and vehicle is a white noise signal of 1000Hz with amplitude of 100 N, we regard W_d as a low-pass filter amplifying signals up to 1000 Hz with a gain of 40 dB.

Performance weighting function

W_e is a bandpass filter amplifying the signal in the frequency range (60-1000Hz) which needs to be controlled. For simplying design, we used a low pass filter instead. It means that we are interested at frequencies below 1000 Hz. The gain is dependent on the problem and will be discussed later.

Control signal weighting function

W_u is used to reduce the controller effort at higher frequencies and ensures that the actuator does not saturate. The frequency shaping typically depends on the actuator's specification. As mentioned above, the actuator only functions up to 1000 Hz.

The weighting functions and plots of W_e, W_u, W_d are shown in the following:

$$W_e = \frac{3 \bullet 2\pi \bullet 250}{s + 2\pi \bullet 250} \qquad (5.24)$$

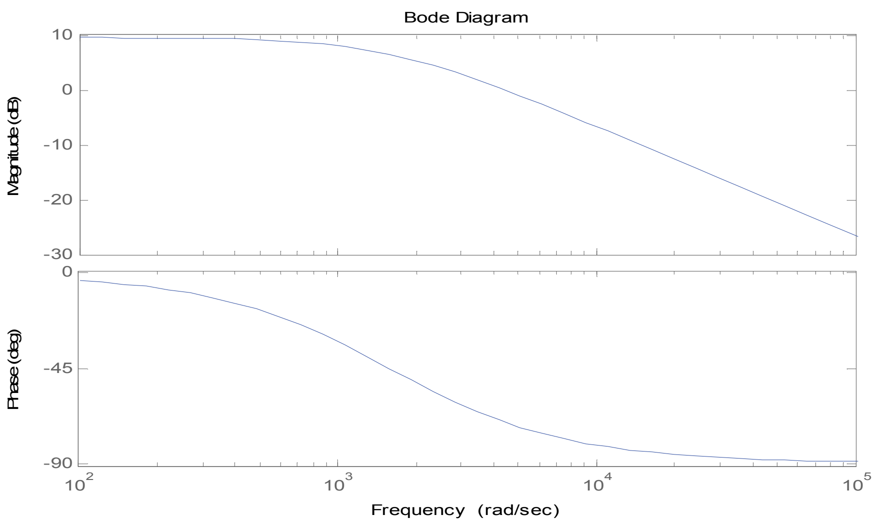

Figure 5-6: Bode Plot of W_e

$$W_u = \frac{30(s+2\bullet\pi\bullet 250)}{s+2\bullet\pi\bullet 250\bullet 100000} \qquad (5.25)$$

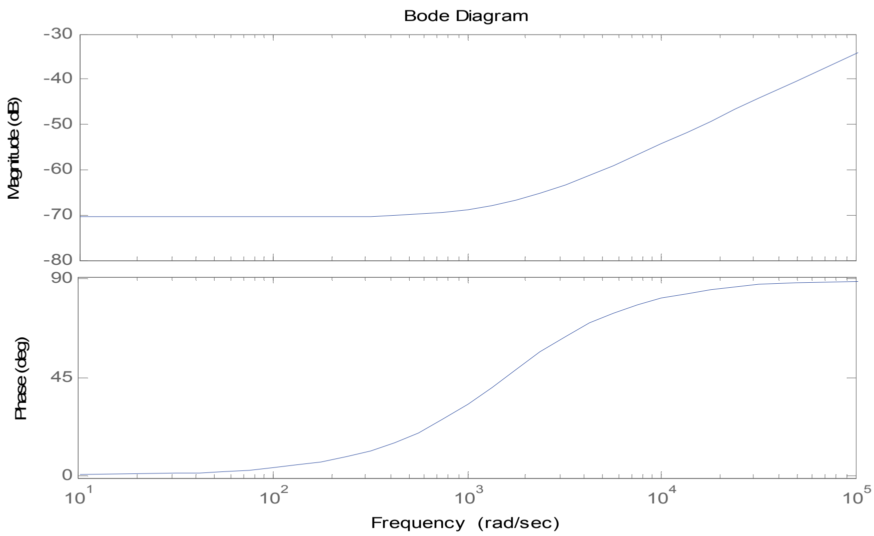

Figure 5-7: Bode Plot of W_u

$$W_d = \frac{30\bullet 2\bullet\pi\bullet 1000}{s+2\bullet\pi\bullet 1000} \qquad (5.26)$$

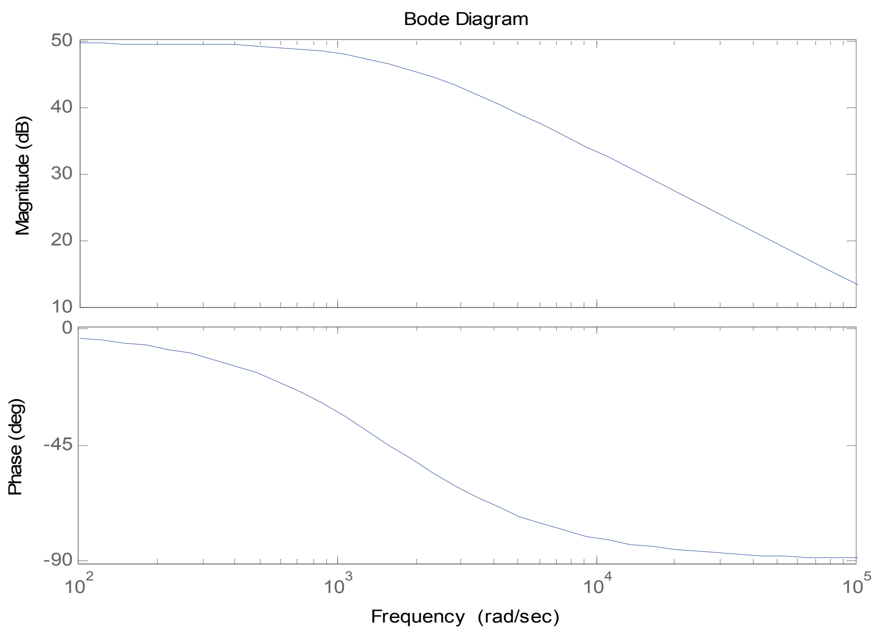

Figure 5-8: Bode Plot of W_d

The weighting functions W_e, W_u, W_d might need to be relaxed by trial-and-error to trade off the performance with robustness.

5.4 Simulations Results of H_∞ and μ-synthesis Controller

Simulink is used to perform the simulations for both test bench and vehicle. The closed and open loop Simulink diagram is illustrated in Figure 5-9.

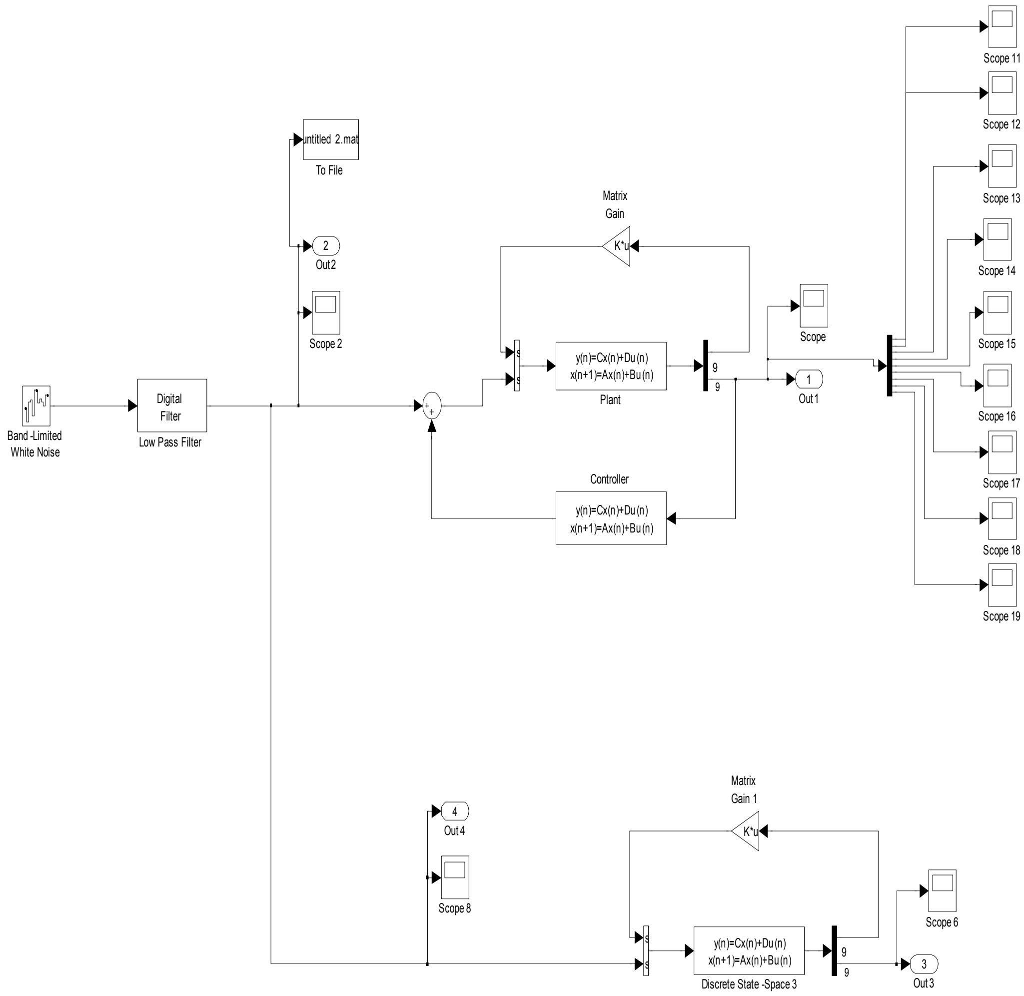

Figure 5-9: Closed and Open Loop System for Simulations

In the simulation model of Figure 5-9, the white noise signal is used as the exciting signal working on the wheel spindle. A low-pass filter follows to suppress the high-frequency noise. So what should be the bandwidth? We determine the cutoff frequency of the low-pass filter by simulating road bumps in the next section.

Road Bump Simulation

Assume a vehicle riding on a rough road with the velocity of 100 km per hour. The vehicle passes over a rectangular bump every 0.125 second; hence, the distance between two bumps is 3.47 m. The height of each bump is 3.16 cm. These data are reasonable in reality.

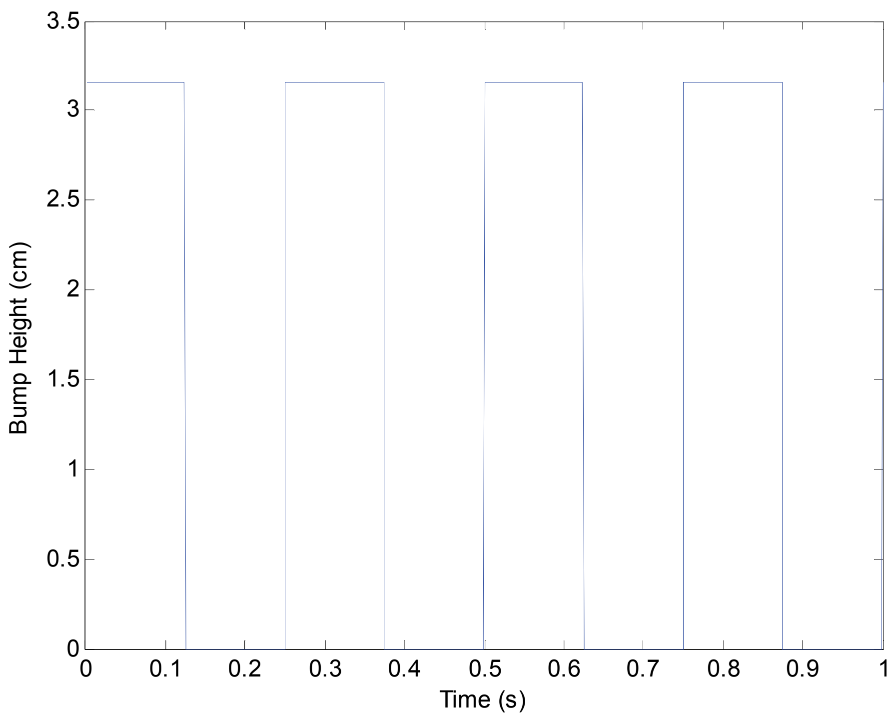

Figure 5-10: Bumps on Rough Road in Time Domain

The signal in Figure 5-10 is shown in the frequency domain in Figure 5-11. From Figure 5-11, we find that most of the power spectrum lies below 170 Hz. Based on this, we designed a low-pass filter which filters out the noise at frequencies higher than 170 Hz, as shown in Figure 5-12.

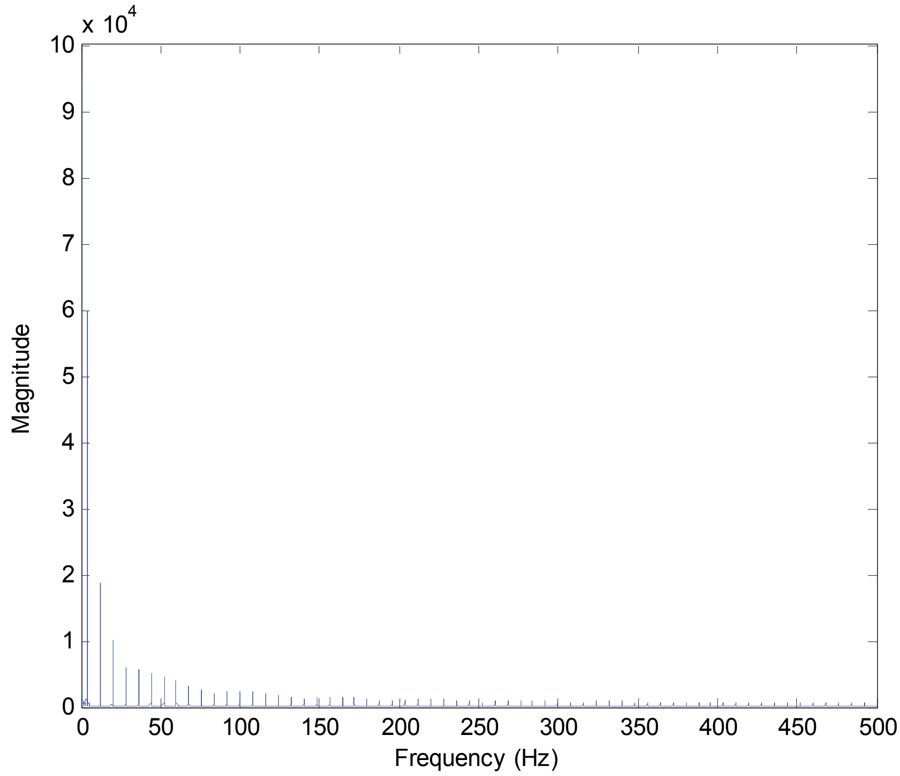

Figure 5-11: Effect of Bumps on Rough Road in the Frequency Domain

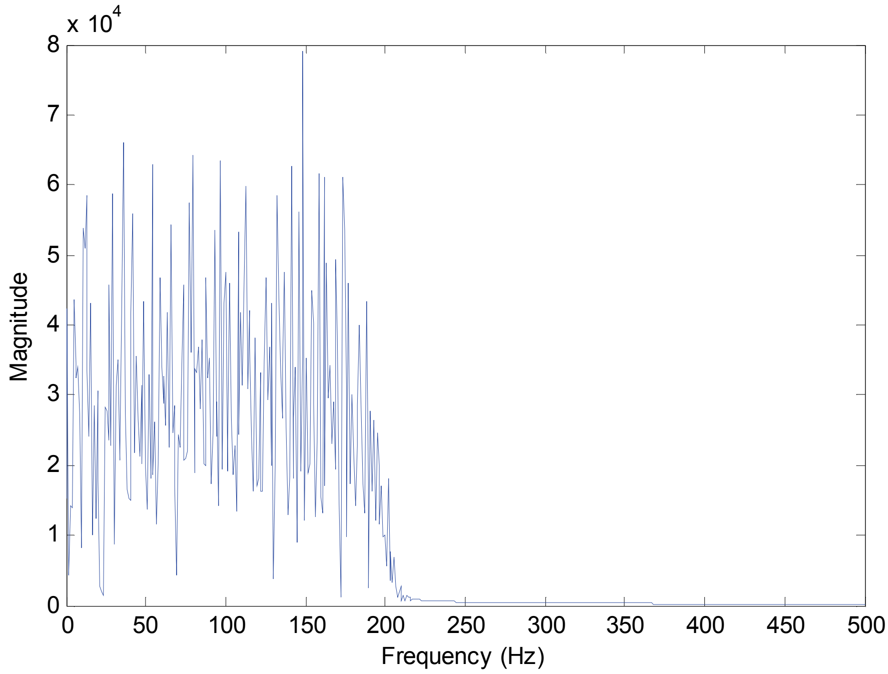

Figure 5-12: Exciting Signal after Lowpass Filtering

5.4.1 Test Bench Performance Analysis

5.4.1.1 Simulation Results in Frequency Domain

For convenience, the simulation results for only three sensors are shown in the following and all other six sensors have similar results.

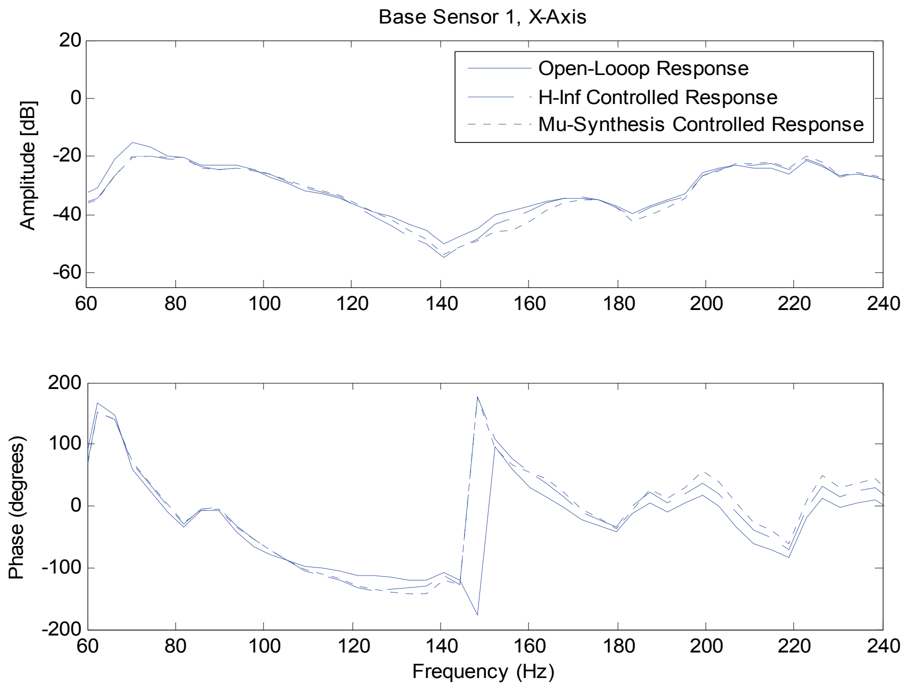

Figure 5-13: Simulation With H_∞ and μ Synthesis Controller for Test Bench (Base Sensor 1, X-Axis)

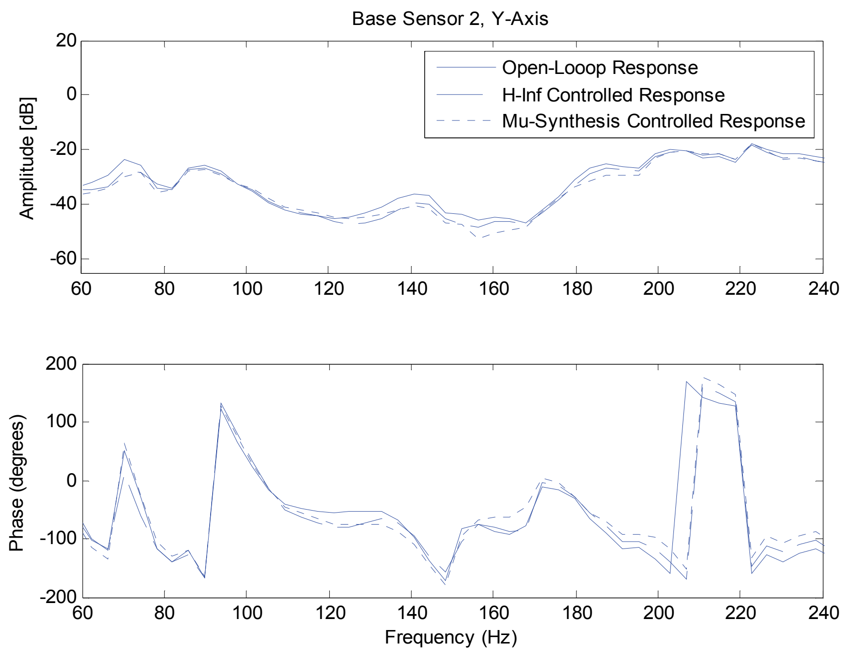

Figure 5-14: Simulation With H_∞ and μ Synthesis Controller for Test Bench (Base Sensor 2, Y-Axis)

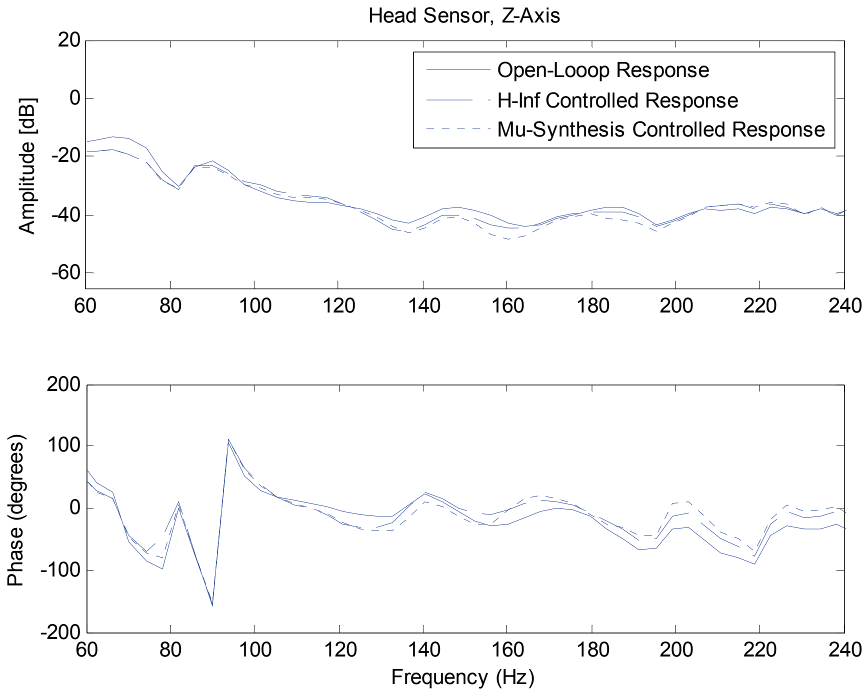

Figure 5-15: Simulation With H_∞ and μ Synthesis Controller for Test Bench (Head Sensor, Z-Axis)

From Figure 5-13, 5-14 and 5-15, we can see that a reduction up to 6 dB is achieved between 60-80Hz for both H_∞ and μ synthesis controller. In the frequency range of 120-200 Hz, the reduction of the H_∞ design is up to 5 dB but the reduction obtained with the μ synthesis design is up to 7 dB. Thus, the μ synthesis controller offers better performance than H_∞. The common drawback of these two controllers is that they are not working for frequency range of 100-120 Hz and over 210 Hz.

5.4.1.2 Simulation Results in Time Domain

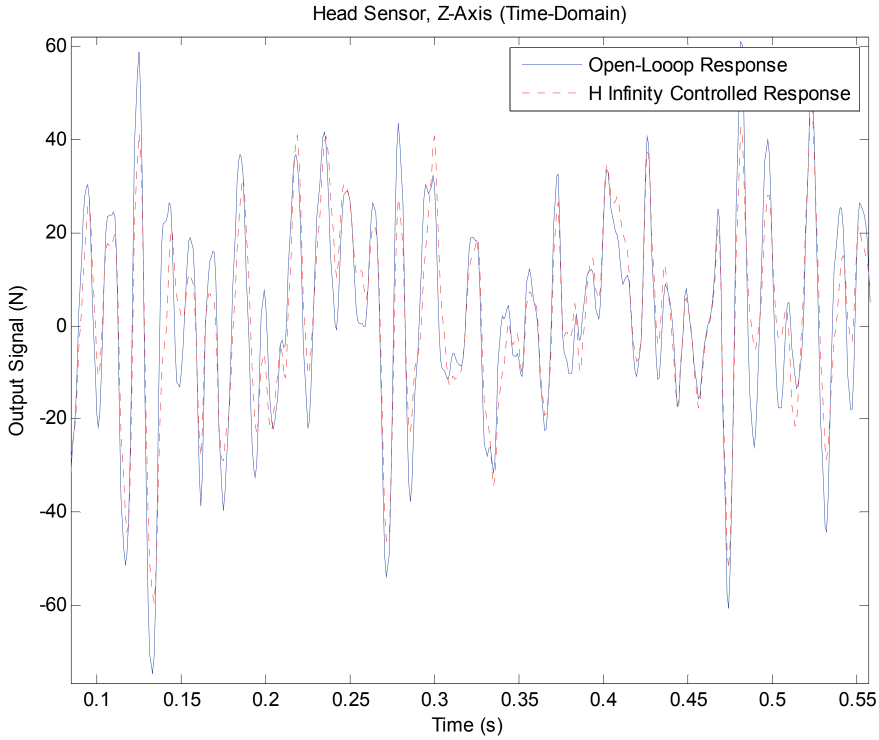

Figure 5-16: Simulation with H Infinity Controller for Test Bench in Time Domain (Head Sensor, Z-Axis)

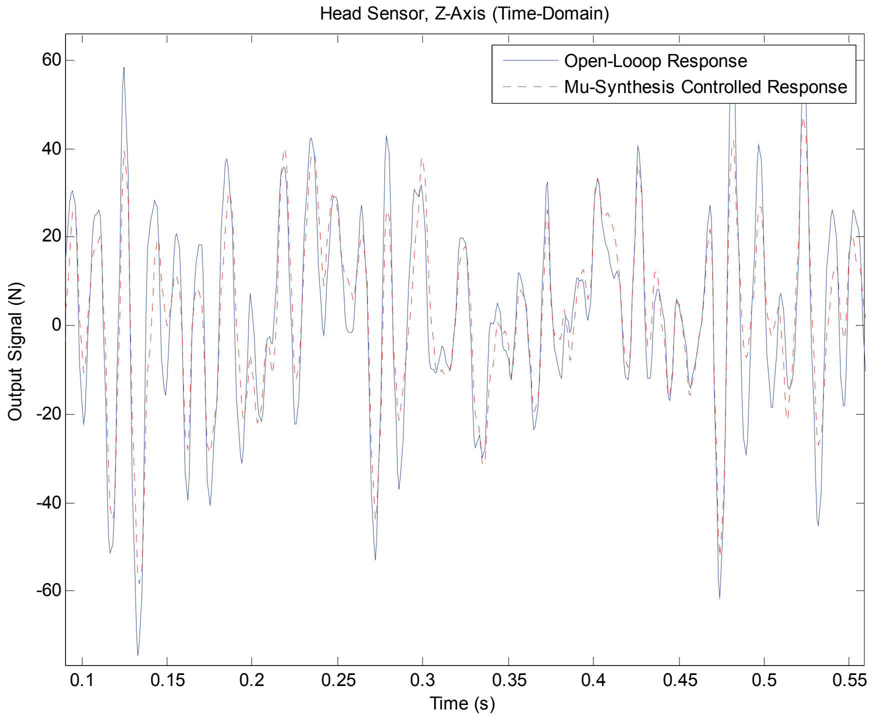

Figure 5-17: Simulation with μ Synthesis Controller for Test Bench in Time Domain (Head Sensor, Z-Axis)

Figure 5-16 and 5-17 show the simulation results in time domain for Head Sensor in Z-Axis. The plots in time domain show the results in all frequencies. Both H-Infinity and μ-Synthesis controllers are able to reduce the vibration amplitude up to 20 N. Our design is based on the frequency domain and only considers the resonant frequencies below 250 Hz so the plot results shown in the figures are not as good as the ones shown in the frequency domain.

5.4.2 Test Vehicle Performance Analysis

5.4.2.1 Simulation Results in Frequency Domain

Like the test bench case, only three simulation results are selected in the following and all other six sensors have similar results.

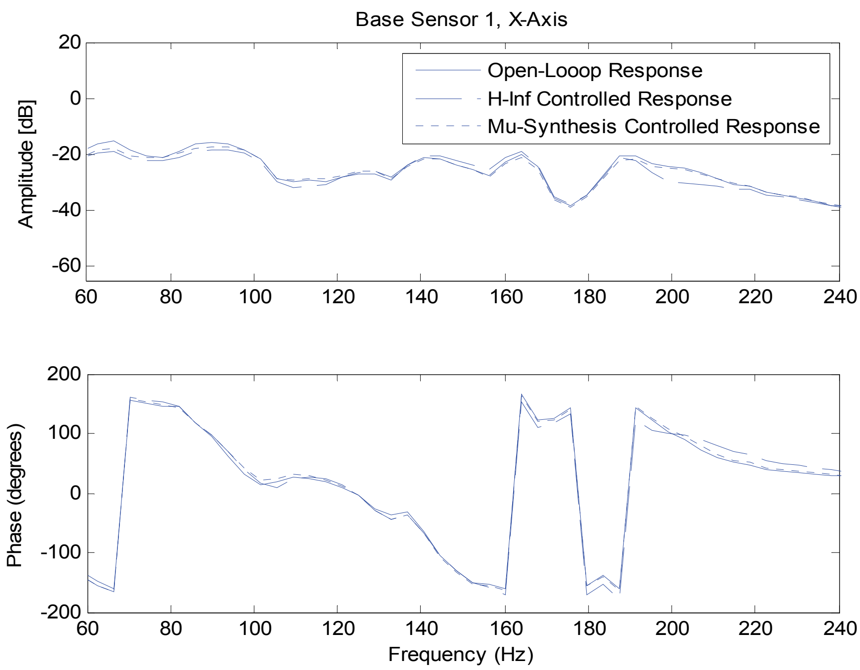

Figure 5-18: Simulation With H_∞ and μ Synthesis Controller for Test Vehicle (Base Sensor 1, X-Axis)

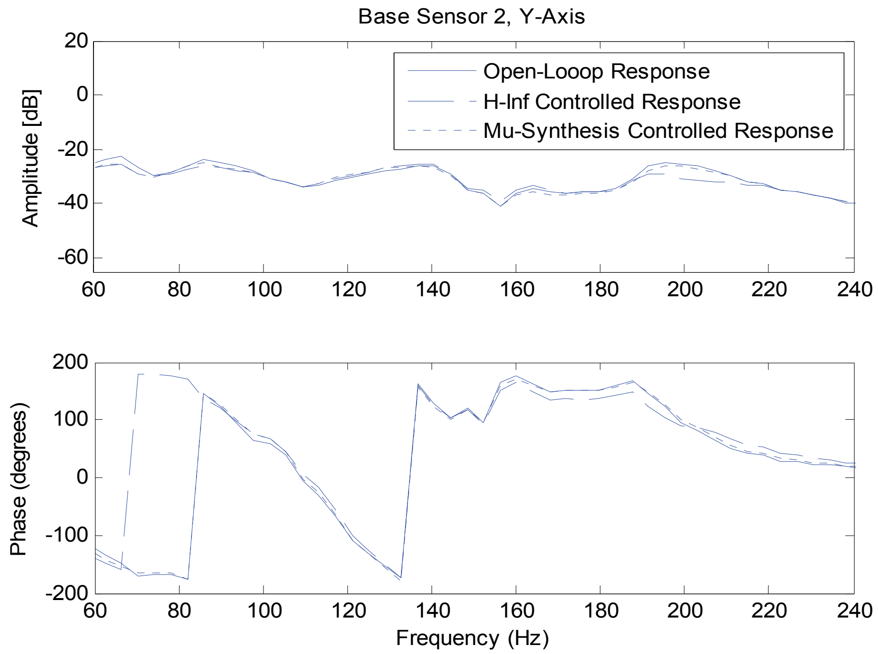

Figure 5-19: Simulation With H_{∞} and μ Synthesis Controller for Test Vehicle (Base Sensor 2, Y-Axis)

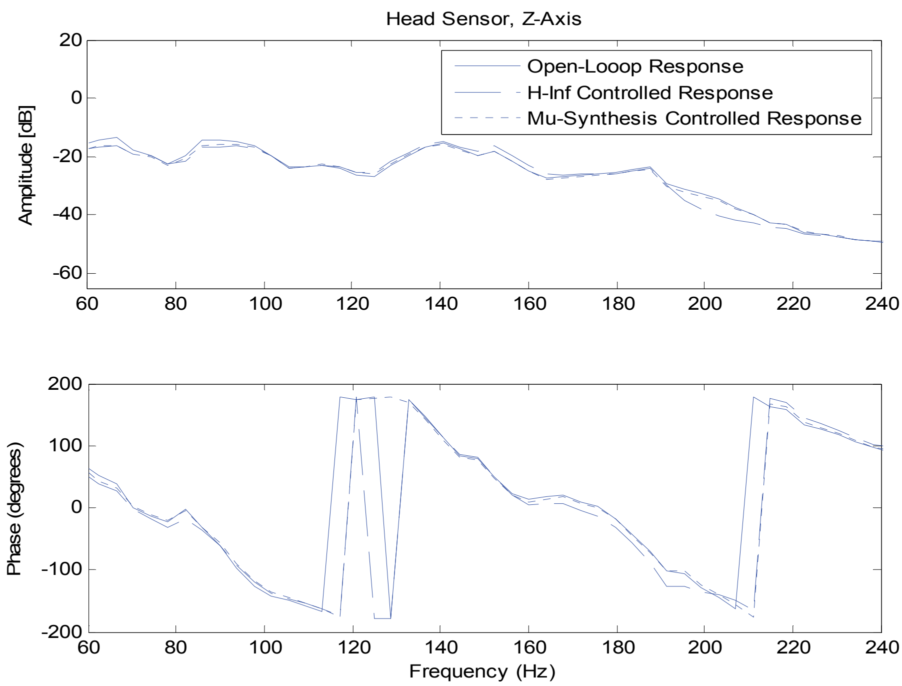

Figure 5-20: Simulation With H_{∞} and μ Synthesis Controller for Test Vehicle (Head Sensor, Z-Axis)

From Figure 5-18, 5-19 and 5-20, we can see that a reduction up to 5 dB is achieved for H_∞ and 3.5 dB for μ synthesis controller between 60-110Hz. Both of these two controllers do not have much effect in the frequency range for 120-190 Hz. Although a reduction of 3.5 dB by the μ synthesis controller is not as good as the reduction of 5 dB by the H_∞ controller, the closed-loop response from the μ synthesis controller can almost be the same or less than the open-loop response. On the other hand, the closed-loop response from H_∞ controller is almost always higher than the open-loop response. This shows again that the closed-loop system designed by μ synthesis is more robust than that of the H_∞ controller design. In the range above 190 Hz, both of the controllers can effectively reduce the magnitude of the frequency response. The common drawback of these two controllers is that they are not working well for the frequency range of 110-140 Hz.

5.4.2.2 Simulation Results in Time Domain

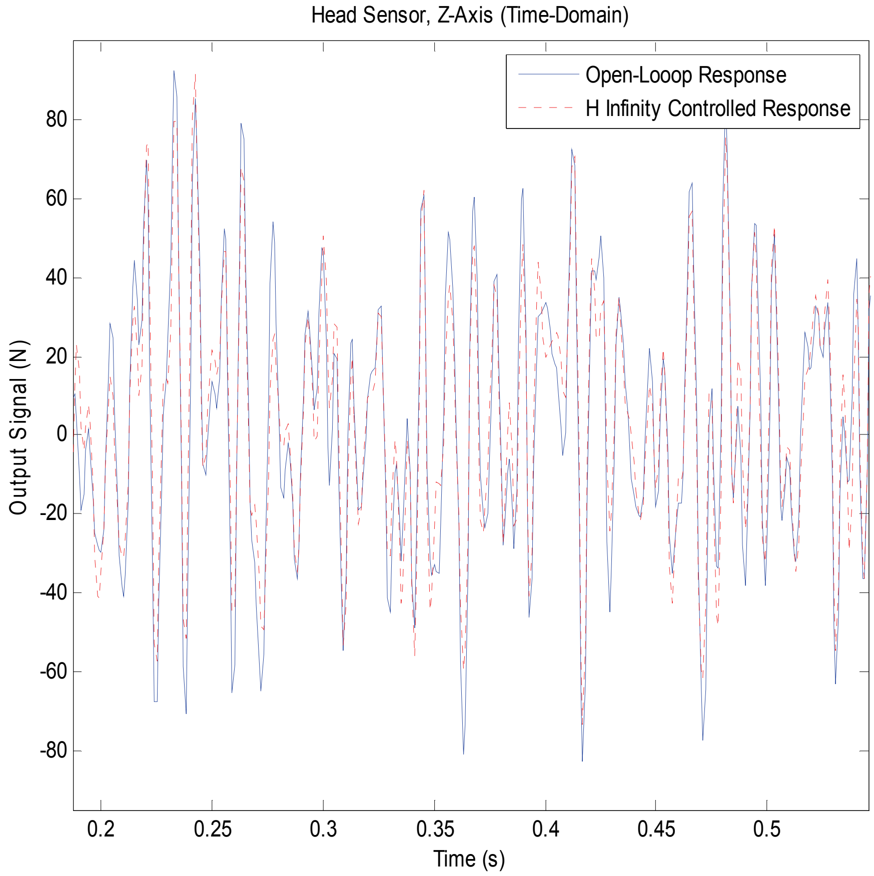

Figure 5-21: Simulation with H Infinity Controller for Test Vehicle in Time Domain (Head Sensor, Z-Axis)

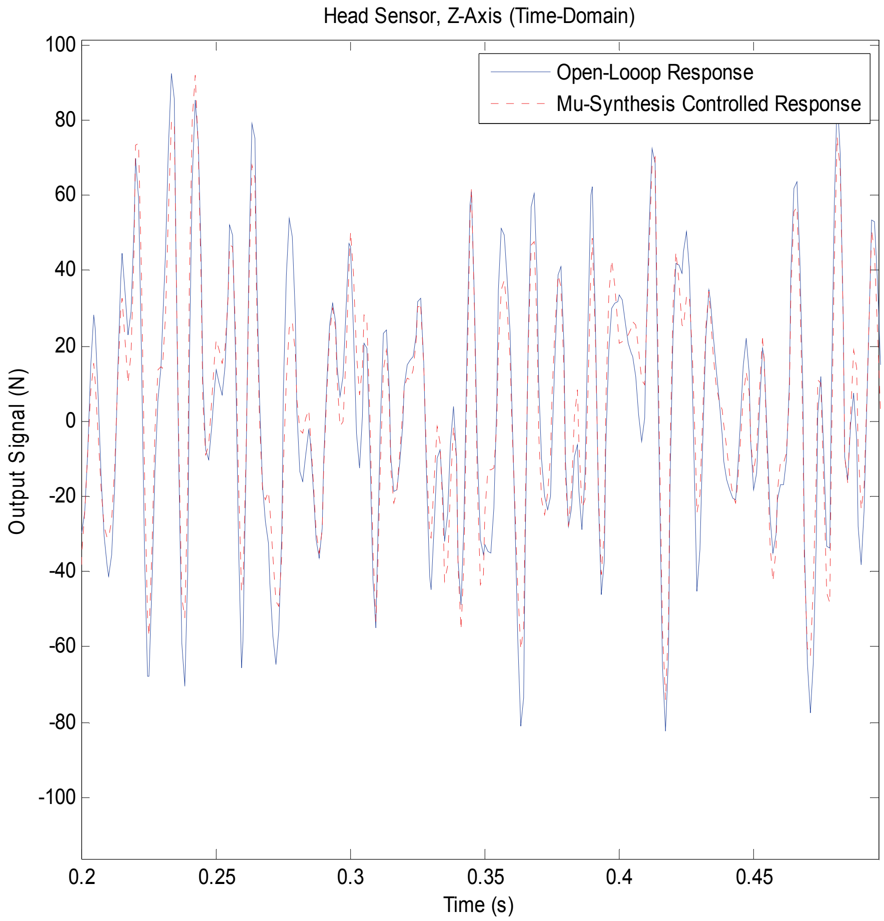

Figure 5-22: Simulation with μ Synthesis Controller for Test Vehicle in Time Domain (Head Sensor, Z-Axis)

Figure 5-21 and 5-22 show the simulation results of the test vehicle in time domain for Head Sensor in Z-Axis. The plots in time domain show the results at all frequencies. Both H-Infinity and μ-Synthesis controllers are able to reduce the vibration magnitude up to 20 N. The same reason as test bench, our design is based on the frequency domain and resonant frequencies below 250 Hz are considered, therefore, the plot results shown on Figures are not as good as the ones shown in the frequency domain. In addition, since the order of the test vehicle dynamics is higher than that of the test bench system, it is hard for the controller to achieve better performance for the test vehicle.

5.4.3 Verifying Robust Control Theory

As we said, a robust control system must trade off performance with robustness due to the plant uncertainties, i.e., the more robust the controller is, the worse the performance it is able to achieve. Thus, we have to find a balance between them in reality. This trade-off is verified by comparing Figure 5-18 with 5-23. These two figures are plotted for the same output sensor of test vehicle, and the difference is that less robustness is required in Figure 5-23. Therefore, it is very easy to find out that Figure 5-23 provides less robustness but better performance. In contrast, Figure 5-18 provides more robust but worse performance. How to choose the balance really depends on the actual control problem.

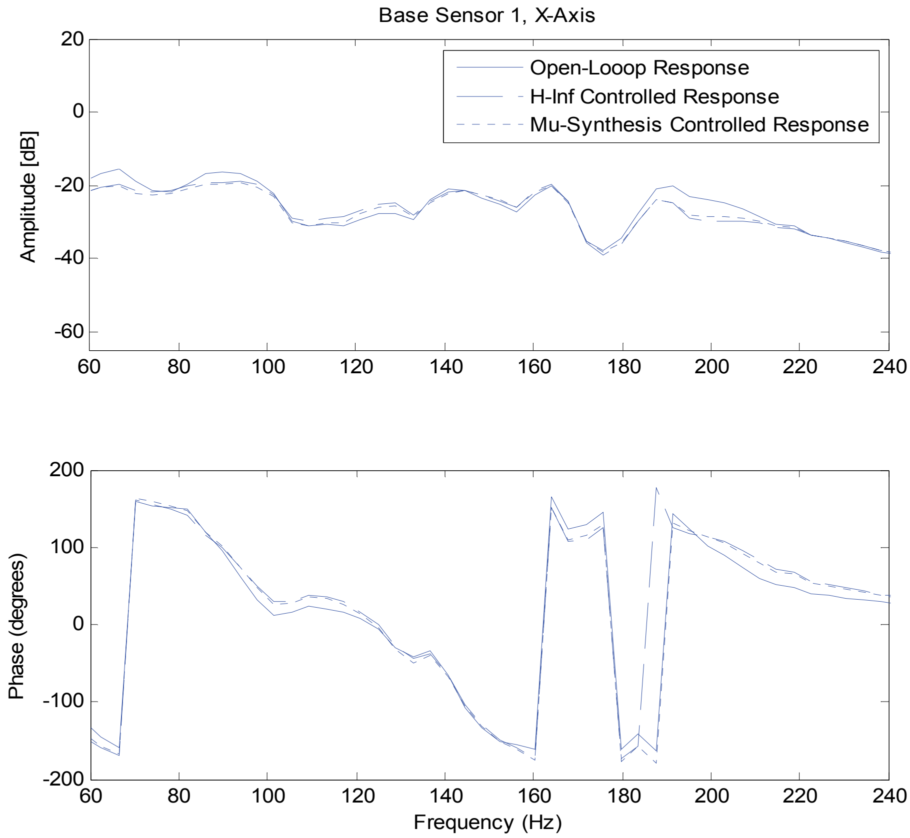

Figure 5-23: Simulation with H_∞ and μ Synthesis Controller for Test Vehicle with a Higher Performance Requirement (Base Sensor 1, X-Axis)

By observing the simulation results, we can also see that the μ-synthesis controller is working better than the H_∞ Controller at most frequencies. However, in some small frequency range, the μ-synthesis controller is working worse than the H_∞ Controller. This may be because our system is large as it is of order 22 for the test bench and 24th order for the test vehicle. Adding the order of the weighting functions, unexpected numerical results may have appeared when doing the D-K iteration process.

Chapter 6 Conclusion and Future Work

6.1 Conclusion

In this thesis, two experimental equipments are modeled by the modal parameter identification. Both of them are single input nine outputs mechanical systems and the nine vibration transmission paths from input to outputs are independent to each other, thus, the modeling is done like nine different single input single output systems. The modal parameters include three parts: natural frequency, damping ratio and output gains for each output. These parameters are computed by minimizing 2-norms of the errors between the models and experimental frequency response.

Parametric uncertainty is applied to model the difference between the model and the physical process. Perturbation of each parameter, i.e. natural frequency ω, damping ratio ζ and output gain R, is obtained by similar method to nominal plant modeling. Afterwards, the nominal model is augmented by including the parametric uncertainties. The goal of this step is to ensure that the augmented model include all of the physical behaviors of the true plant.

Two kinds of robust controllers have been designed to achieve both robustness and performance requirements. The first controller is designed by H-infinity technique and computed by the Matlab command 'hinfsyn' from Matlab toolbox. The second one is designed through μ-synthesis technique and computed by

Matlab command 'dkit'. An important procedure in this step is to find proper weighting functions to describe performance specifications, represent the frequency contents of disturbances and constrain the magnitude of the input signals for actuator to prevent actuator saturation. Usually, the weighting functions can be determined once, and need many trials to release and find a balance between robustness and performance.

Simulation results in both frequency and time domains are shown by running Simulink in Matlab. For test bench, the H-infinity controller can reduce the magnitude of vibrations up to 5 dB and the reducing of μ-synthesis controller is up to 7 dB in frequency domain. As expected, μ-synthesis controller can achieve a better performance than H-infinity controller. For test vehicle, a reduction up to 5 dB is achieved for H_∞ and 3.5 dB for μ-synthesis controller between 60-110Hz. Since the order for test vehicle is very high and some unexpected results could appear when doing D-K iteration process. This is one of the reasons which make the μ-synthesis controller have the worse performance than H-infinity controller. However, Figures 5-18 and 5-23 also show that μ-synthesis controller can achieve a better performance by adjusting the weighting functions but the disadvantage is that the controller becomes less robustness. In time domain, the performance of both H-infinity and μ-synthesis controller is not as good as that in frequency domain since the design is based on the frequency domain and only the low frequency range is considered.

6.2 Future Work

Modeling and controller design for other three suspension systems should be finished. Since the structure of back two suspensions are different from the front ones, based on my experience, more modeling work might be needed for them.

Disturbance and control signals are co-located in this thesis, however, this is not realistic and more ideal model is to use independent actuators for each suspensions. In this case, new transmission paths from input to actuator to output sensors should be modeled and the G(s) in Figure 5-5 should be a transfer matrix with a dimension two by one.

Once the experimental car is finished setting up, the experiments can also be done to further verify the effectiveness of controllers on the real system. As far as I can think, the factor of time delay must be considered.

This thesis proves that H-infinity and μ-synthesis robust controllers can achieve an acceptable tradeoff between robustness and performance for vehicle suspension systems. However, it still needs more efforts to make them work more effectively on the real system.

REFERENCES

[1] Fuller, C.R.; von Flotow, A.H., "Active control of sound and vibration," *Control Systems Magazine, IEEE* , vol.15, no.6, pp.9-19, Dec 1995

[2] J.N. Juang and Richard S. Pappa, *Journal of Guidance, Control and Dynamics* (1985) 8(5), 620-627. An Eigensystem Realization Algorithm for Modal Parameter Identification and Model Reduction.

[3] Pappa, R. S., James, G. H., and Zimmerman, D. C. (1998). "Autonomous modal identificationof the space shuttle tail rudder." AIAA Journal of Guidance, Control, and Dynamics, 35(2),163–169.

[4] Pappa, R. S. and Elliott, K. B. (1993). "Consistent-mode indicator for the eigensystem realization algorithm." AIAA Journal of Guidance, Control, and Dynamics, 16(5), 852–858.

[5] Bejarano Rodriquez, Fernando Andres (2008). Crack identification of a rotating shaft with integrated wireless sensors. M.S. dissertation, University of Puerto Rico, Mayaguez (Puerto Rico), United States -- Puerto Rico. Retrieved April 17, 2009, from Dissertations & Theses: Full Text database. (Publication No. AAT 1451270).

[6] Narkis Y., "Identification of Crack Location in Vibrating Simply Supported Beams'',
Journal of Sound and Vibration, 172(4), pp.549-558, 1994.

[7] Kemin Zhou and John C. Doyle. *Essentials of Robust Control*. Prentice Hall, Upper Saddle River, New Jearsey, 1998.

[8] Robertson, S.S.; Leithead, W.E.; O'Reilly, J., "Nyquist/Bode design for multivariable systems with parametric uncertainty," *Robust Control: Theory, Software and Applications (Digest No: 1997/380), IEE Colloquium on* , vol., no., pp.3/1-3/4, 17 Oct 1997

[9] W.E. Leithead, S.S. Robertson, and J. O'Reilly. Design of controllers within the framework of ICAD. In *SjvnposiLim or1 Quantitative Feedback Theory and Other Frequency-Based Methods and Applications,* pages 219-225, Glasgow, U.K., August 1997.

[10] W.E. Leithead, S.S. Robertson, and J. O'Reilly. The relationship of QFT to ICAD. In *Symposium on Quarzriratiw Feedback Theory and Other Frequency-Based Methods and Applications,* pages *5 5 4 2 ,* Glasgow, U.K., August 1997

[11] Indra Narayan Kar; Seto, K.; Doi, F., "Multimode vibration control of a flexible structure using H_∞-based robust control," *Mechatronics, IEEE/ASME Transactions on* , vol.5, no.1, pp.23-31, Mar 2000.

[12] Sato, M., and Suzuki, M., "Vibration Control of Flexible Structures Using a Combined H1 Filter Approach," *Journal of Guidance, Control, and Dynamics*, Vol. 19, No. 5, 1996, pp. 1000–1006.

[13] Fujita, M.; Namerikawa, T.; Matsumura, F.; Uchida, K., "μ-synthesis of an electromagnetic suspension system," *Automatic Control, IEEE Transactions on* , vol.40, no.3, pp.530-536, Mar 1995

[14] Moser, A.N., "Designing controllers for flexible structures with H-infinity/μ-synthesis," *Control Systems Magazine, IEEE* , vol.13, no.2, pp.79-89, Apr 1993

[15] Jolicoeur, Marie-Pierre (2006). Model identification of a car suspension testbed for robust vibration control. M.Eng. dissertation, McGill University (Canada), Canada. Retrieved April 24, 2009, from Dissertations & Theses @ McGill University database. (Publication No. AAT MR24971).

[16] Anders Helmersson. Methods for Robust Gain Scheduling. PhD thesis, Linkoping University, Sweden, Department of Electrical Engineering, 1995.

[17] Vanreusel, Stephen (2006). Identification and multivariable feedback control of the vibration dynamics of an automobile suspension. M.Eng. dissertation, McGill University (Canada), Canada. Retrieved April 24, 2009, from Dissertations & Theses @ McGill University database. (Publication No. AAT MR25015).

[18] Benoit Boulet. Robust Control Systems, Course Notes, 2007.